

## meso-Aryl-Substituted Subporphyrins: Synthesis, Structures, and Large Substituent Effects on Their Electronic Properties

Yasuhide Inokuma,<sup>†</sup> Zin Seok Yoon,<sup>‡</sup> Dongho Kim,<sup>\*,‡</sup> and Atsuhiko Osuka<sup>\*,†</sup>

Contribution from the Department of Chemistry, Graduate School of Science, Kyoto University, Sakyo-ku, Kyoto 606-8502, Japan, and Department of Chemistry and Center for Ultrafast Optical Characteristics Control, Yonsei University, Seoul 120-749, Korea

Received December 28, 2006; E-mail: osuka@kuchem.kyoto-u.ac.jp; dongho@yonsei.ac.kr

**Abstract:** Two synthetic methods of meso-aryl-substituted subporphyrins have been developed by means of the reaction of pyridine-tri-*N*-pyrrolylborane with a series of aryl aldehydes. One method relies on the condensation under Adler conditions with chloroacetic acid in refluxing 1,2-dichlorobenzene to afford subporphyrins in 1.1–3.2%, and the other is a two-step reaction consisting of the initial treatment of the two substrates with trifluoroacetic acid at 0 °C followed by air-oxidation in refluxing 1,2-dichlorobenzene to provide subporphyrins in up to 5.6% yield. <sup>1</sup>H NMR studies indicate that phenyl and sterically unhindered substituents at the meso position of subporphyrins rotate rather freely even at –90 °C, whereas the rotation of meso-2,4,6-trimethoxyphenyl substituents is strictly prohibited even at 130 °C. The structures of six subporphyrins have been revealed by X-ray crystallographic analysis to be all cone-shaped tripyrrolic macrocycles. Dihedral angles of meso-phenyl and sterically unhindered aryl substituents to the subporphyrinic core are rather small (38.3–55.7°) compared to those of porphyrin analogues, whereas those of meso-2,4,6-trimethoxy-substituted subporphyrins are large (68.7–75.7°). These rotational features of the meso-aryl substituents lead to their large influences on the electronic properties of subporphyrins, as seen for 4-nitrophenyl-substituted subporphyrin **14e** that exhibits perturbed absorption and fluorescence spectra, depending upon solvents. Large solvent-polarity dependence of the fluorescence of **14e** suggests the charge-transfer character for its excited state. Electrochemical and theoretical studies are performed to understand the electronic properties. Overall, meso-aryl-substituted subporphyrins are promising chromophores in future functional devices.

### Introduction

Expanded porphyrins that have larger conjugated pyrrolic macrocycles than porphyrin **1** exhibit unprecedented chemical reactivities, low-energy absorption bands that reach well into the far-infrared region, extremely large two-photon absorption cross sections, multiple metal ion coordination, and facile aromatic/antiaromatic switches upon two-electron redox in their electronic  $\pi$ -systems.<sup>1–3</sup> These promising properties led to a considerable upsurge in the development of these new porphyrinoid families. In sharp contrast, the chemistry of contracted porphyrins has remained quite unexplored except those of corroles **2** that have a one-methine-bridge-missing porphyrinic skeleton.<sup>4</sup>

This situation contrasts markedly to that of phthalocyanines, in that both ring-expanded superphthalocyanines and ring-

contracted subphthalocyanines have been known and extensively studied so far. Superphthalocyanine **3** with an aromatic  $22\pi$ -electronic circuit was synthesized by the condensation of

<sup>†</sup> Kyoto University.

<sup>‡</sup> Yonsei University.

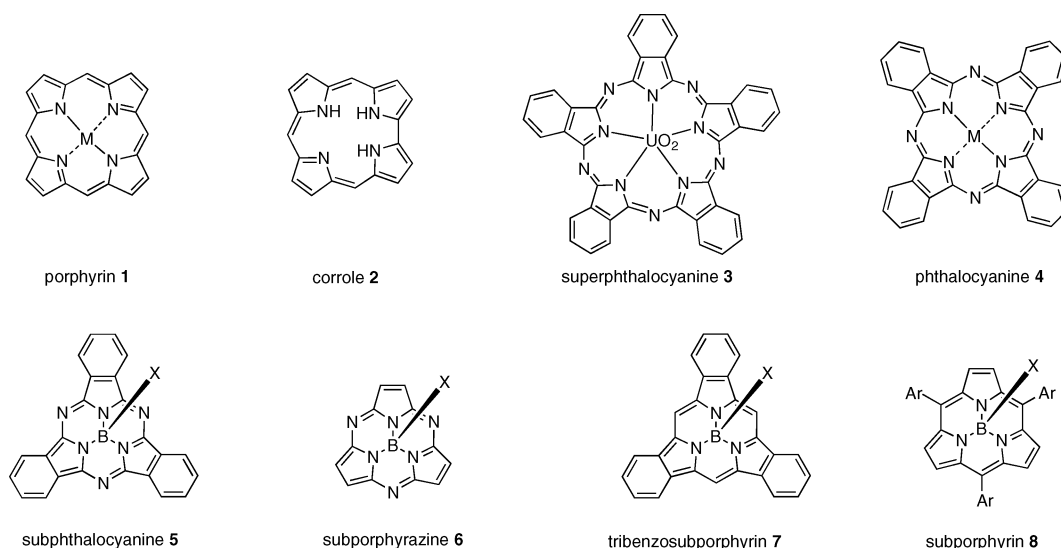
(1) (a) Franck, B.; Nonn, A. *Angew. Chem., Int. Ed. Engl.* **1995**, *34*, 1795–1811. (b) Jasat, A.; Dolphin, D. *Chem. Rev.* **1997**, *97*, 2267–2340. (c) Sessler, J. L.; Gebauer, A.; S. J. Weghorn, S. J. In *The Porphyrin Handbook*; Kadish, K. M.; Smith, K. M., Guillard, R., Eds.; Academic Press: San Diego, 1999; Vol. 2, pp 55–124. (d) Lash, T. D. *Angew. Chem., Int. Ed.* **2000**, *39*, 1763–1767. (e) Furuta, H.; Maeda, H.; Osuka, A. *Chem. Commun.* **2002**, 1795–1804. (f) Sessler, J. L. D. Seidel, D. *Angew. Chem., Int. Ed.* **2003**, *42*, 5134–5175. (g) Ghosh, A. *Angew. Chem., Int. Ed.* **2004**, *43*, 1918–1931. (h) Chadrashekar, T. K.; Venkatraman, S. *Acc. Chem. Res.* **2003**, *36*, 676–691.

(2) (a) Sessler, J. L.; Cyr, M. J.; Lynch, V.; McGhee, E.; Ibers, J. A. *J. Am. Chem. Soc.* **1990**, *112*, 2810–2813. (b) Sessler, J. L.; Weghorn, S. J.; Lynch, V.; Johnson, M. R. *Angew. Chem., Int. Ed. Engl.* **1994**, *33*, 1509–1512. (c) Vogel, E.; Bring, M.; Fink, J.; Rosen, D.; Schmickler, H.; Lex, J.; Chan, K. W. K.; Wu, Y. D.; Platter, D. A.; Nendel, M.; Houk, K. N. *Angew. Chem., Int. Ed. Engl.* **1995**, *34*, 2511–2514. (d) Bring, M.; Dietrich, H.-J.; Dörr, J.; Hohlneicher, G.; Lex, J.; Jux, N.; Pütz, C.; Roeb, M.; Schmickler, H.; Vogel, E. *Angew. Chem., Int. Ed.* **2000**, *39*, 1105–1108. (e) Vogel, E.; Michels, M.; Zander, L.; Lex, J.; Tuzum, N. S. Houk, K. N. *Angew. Chem., Int. Ed.* **2003**, *42*, 2857–2862. (f) Sestune, J.; Maeda, S. *J. Am. Chem. Soc.* **2000**, *122*, 12405–12406. (g) Sprutta, N.; Latos-Grażyński, L. *Chem. Eur. J.* **2001**, *7*, 5099–5112. (h) Hung, C. H.; Jong, J. P.; Ho, M. Y.; Lee, G. H.; Peng, S. M. *Chem. Eur. J.* **2002**, *8*, 4542–4548. (i) Anand, V. G.; Pushpan, S. K.; Venkatraman, S.; Dey, A.; Chandrashekar, T. K.; Joshi, B. S.; Roy, R.; Teng, W.; Senge, K. R. *J. Am. Chem. Soc.* **2001**, *123*, 8620–8621. (j) Krivokapic, A.; Cowley, A. R.; Anderson, H. L. *J. Org. Chem.* **2003**, *68*, 1089–1096. (k) Xu, L.; Ferrence, G. M.; Lash, T. D. *Org. Lett.* **2006**, *8*, 5113–5116.

(3) (a) Neves, M. G. P. M. S.; Martins, R. M.; Tomé, A. C.; Silvestre, A. J. D.; Silva, A. M. S.; Félix, V.; Drew, M. G. B.; Cavaleiro, J. A. S. *Chem. Commun.* **1999**, 385–386. (b) Shin, J. Y.; Furuta, H.; Yoza, K.; Igarashi, S.; Osuka, A. *J. Am. Chem. Soc.* **2001**, *123*, 7190–7191. (c) Suzuki, M.; Osuka, A. *Org. Lett.* **2003**, *5*, 3943–3946. (d) Shimizu, S.; Shin, J. Y.; Furuta, H.; Ismael, R.; Osuka, A. *Angew. Chem., Int. Ed.* **2003**, *42*, 78–82. (e) Shimizu, S.; Aratani, N.; Osuka, A. *Chem. Eur. J.* **2006**, *12*, 4909–4918.

(4) (a) Paollesse, R. In *The Porphyrin Handbook*; Kadish, K. M., Smith, K. M., Guillard, R., Eds.; Academic Press: San Diego, 1999; Vol. 2, pp 201–232. (b) Erbem, C.; Will, S.; Kadish, K. M. In *The Porphyrin Handbook*; Kadish, K. M., Smith, K. M., Guillard, R., Eds.; Academic Press: San Diego, 1999; Vol. 2, pp 233–300.

Chart 1



phthalonitrile in the presence of a uranyl ion template.<sup>5</sup> It was shown that the stability of **3** relied on the central uranyl ion with long N–U bond distances ( $\sim 2.5$  Å) and the removal of uranyl ion led to its smooth decomposition with concurrent formation of phthalocyanine **4**. Since the serendipitous discovery by Meller and Ossko in 1972,<sup>6</sup> subphthalocyanines **5**<sup>7</sup> have been widely investigated with regard to dyes, fluorophores,<sup>8</sup> anion-sensing agents,<sup>9</sup> second-order nonlinear optical properties,<sup>10</sup> and as a useful construction kit for curved supramolecular assembly.<sup>11</sup> Subporphyrazines **6** are also important ring-contracted phthalocyanines.<sup>12</sup> The crucial role of the boron template in the preparations of **5** and **6** has now been widely recognized, and these ring-contracted phthalocyanines exist only as their boron(III) complexes, which exhibit blue-shifted absorption bands and have bowl-shaped structure with N–B distances of  $\sim 1.5$  Å. Interestingly, subphthalocyanines have been shown to react with phthalonitriles or diiminoisoindoles to provide corresponding A<sub>3</sub>B-type phthalocyanines with a loss of the central boron(III) ion. This process is useful for the synthesis of non-symmetrical phthalocyanines.<sup>13</sup>

Subporphyrin(1.1.1) that is regarded as a genuine ring-contracted porphyrin may serve as a benchmark for understanding C<sub>3</sub> symmetric porphyrinic  $\pi$ -system as well as a promising chromophore for various functions but has been synthesized only quite recently. We reported the synthesis of [14]tribenzosubporphyrin(1.1.1) (**7**) via high-temperature or microwave-promoted condensation of isoindolinone-3-acetic acid with a boron(III) template as the first example of subporphyrin. Tribenzosubporphyrins show bowl-shaped structures with variable bowl depth, and exhibit Soret bands around 355 nm, Q-bands around 480–515 nm, and green emission at 517 nm with fluorescence quantum yield of 0.41. In next step, we have attempted to synthesize *meso*-triaryl-substituted [14]subporphyrins(1.1.1) **8**, since they are more versatile with regard to *meso* substituents, which is favorable for future applications. Quite recently, Kobayashi et al. reported the synthesis of several *meso*-aryl subporphyrins using tri-*N*-pyrrolylborane (**9**) under Adler conditions.<sup>14</sup> In this paper, we report reliable synthetic methods for *meso*-aryl-substituted subporphyrins **8** from pyridine–tri-*N*-pyrrolylborane (**12**) as a stable and easily handled precursor.<sup>15</sup> The structural, optical, electrochemical, and photoexcited prop-

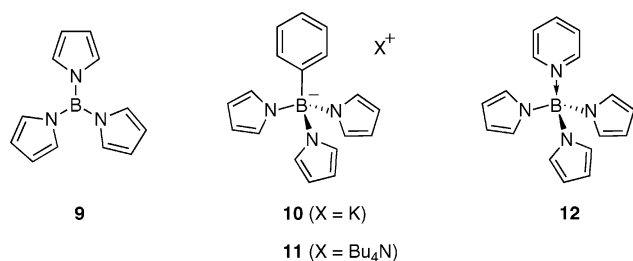
erties of subporphyrins are also reported. It is interesting to note that the  $\pi$ -electronic network of subporphyrin is analogous to those of corranulene and sumanene<sup>16</sup> with respect to bowl-shaped  $\pi$ -conjugation. Therefore, *meso*-aryl-substituted subporphyrins may be a promising tool for construction of curved  $\pi$ -conjugated molecules such as molecular spheres, molecular tubes, molecular belts, and so on (Chart 1).

## Results and Discussion

**Synthesis.** An indispensable and crucial requisite for construction of tripyrrolic macrocycles is a centrally coordinated boron(III) ion, since all such molecules exist as boron-chelated complexes, including subphthalocyanines, subporphyrazines, tribenzosubporphyrin, and *meso*-aryl-substituted subporphyrins. Boron(III) salt serves as an effective templating agent, and in the tripyrrolic macrocycles, the central boron(III) atom seems to mitigate steric repulsion of the inner pyrrolic protons. Thus,

- (5) (a) Bloor, J. E.; Schlabit, J.; Walden, C. C.; Demerdac, A. *Can. J. Chem.* **1964**, *42*, 2201. (b) Marks, T. J.; Stojakovic, D. R. *J. Am. Chem. Soc.* **1978**, *100*, 1695–1705. (c) Day, V. W.; Marks, T. J.; Wachter, W. A. *J. Am. Chem. Soc.* **1975**, *97*, 4519–4527.
- (6) Meller, A.; Ossko, A. *Monatsh. Chem.* **1972**, *103*, 150–155.
- (7) Claessens, C. G.; Gonzalez-Rodriguez, D.; Torres, T. *Chem. Rev.* **2002**, *102*, 835–853.
- (8) (a) González-Rodríguez, D.; Torres, T.; Guldi, D. M.; Rivera, J.; Echegoyen, L. *Org. Lett.* **2002**, *4*, 335–338. (b) González-Rodríguez, D.; Torres, T.; Guldi, D. M.; Rivera, J.; Herranz, M. A.; Echegoyen, L. *J. Am. Chem. Soc.* **2004**, *126*, 6301–6313.
- (9) (a) Ros-Lis, J. V.; Martínez-Mañez, R.; Soto, J. *Chem. Commun.* **2005**, 5260–5262. (b) Xu, S.; Chen, K.; Tian, H. *J. Mater. Chem.* **2005**, *15*, 2676–2680.
- (10) (a) Sastre, A.; Torres, T.; Díaz-García, M. A.; Agulló-López, F.; Dhenaut, C.; Brasselet, S.; Ledoux, I.; Zyss, J. *J. Am. Chem. Soc.* **1996**, *118*, 2746–2747. (b) Rojo, G.; Hierro, A.; Díaz-García, M. A.; Agulló-López, F.; del Ray, B.; Sastre, A.; Torres, T. *Appl. Phys. Lett.* **1997**, *70*, 1802–1804.
- (11) Claessens, C. G.; Torres, T. *J. Am. Chem. Soc.* **2002**, *124*, 14522–14523.
- (12) (a) Rodríguez-Morgade, M. S.; Esperanza, S.; Torres, T.; Barberá, J. *Chem. Eur. J.* **2005**, *11*, 354–360. (b) Rauschnabel, J.; Hanack, M. *Tetrahedron Lett.* **1995**, *36*, 1629–1632.
- (13) (a) Kobayashi, N.; Kondo, R.; Nakajima, S.; Osa, T. *J. Am. Chem. Soc.* **1990**, *112*, 9640–9641. (b) Sastre, A.; Torres, T.; Hanack, M. *Tetrahedron Lett.* **1995**, *36*, 8501–8504.
- (14) Kobayashi, N.; Takeuchi, Y.; Matsuda, A. *Angew. Chem., Int. Ed.* **2007**, *46*, 758–760.
- (15) Inokuma, Y.; Osuka, A. *The 10th International KYOTO Conference on New Aspects of Organic Chemistry*; The Kinki Chemical Society: Kyoto, Japan, 2006; Poster A-129.
- (16) (a) Scott, L. T. *Angew. Chem., Int. Ed.* **2004**, *43*, 4994–5007. (b) Sakurai, H.; Daiko, T.; Hirao, T. *Science* **2003**, *301*, 1878. (c) Sakurai, H.; Daiko, T.; Sakane, H.; Amaya, T.; Hirao, T. *J. Am. Chem. Soc.* **2005**, *127*, 11580–11581.

Chart 2



subpyrrolylborane,<sup>17</sup> tripyrrolylborane (1.1.3), and (2.2.2) derivatives<sup>2j,18</sup> are known as free-base tripyrrolic macrocycles.

In the first place, effective boron templates were searched for subporphyrin synthesis under the Adler and Lindsey conditions used for porphyrin synthesis. Boron trichloride, which is one of the most common templates for subphthalocyanine synthesis, was found entirely not effective for subporphyrin synthesis, because it merely induced extensive polymerization of pyrroles or pyrrolic precursors. Other boron compounds such as B(OMe)<sub>3</sub>, B(OiPr)<sub>3</sub>, and phenyl boronic acid were also not effective for subporphyrin synthesis. Tripyrrolylborane **9**, which was used for the synthesis of *meso*-aryl-substituted subporphyrins by Kobayashi et al.,<sup>14</sup> may be a promising precursor for subporphyrin synthesis. However, as reported previously,<sup>19</sup> **9** is very sensitive to oxygen and moisture, and its manipulation must be done under dry and inert atmosphere. Additionally, pure crystalline solids of **9** obtained by sublimation have low solubility in CH<sub>2</sub>Cl<sub>2</sub> and CHCl<sub>3</sub>. Indeed, *meso*-aryl substituted subporphyrins were formed only in a trace amount from the reaction of **9** with aryl aldehydes in our hands. Thus, we examined other tri-*N*-pyrrolylborane derivatives **10**–**12**<sup>20</sup> for subporphyrin synthesis (Chart 2).

Potassium phenyltri-*N*-pyrrolylborate (**10**) is quite stable toward water and oxygen, but it has low solubility in common organic solvents. When reacted with aryl aldehyde in a refluxing mixture of toluene and acetic acid under aerobic conditions, **10** was gradually dissolved, but subporphyrin **13** was formed only in a trace amount. Tetrabutylammonium phenyltri-*N*-pyrrolylborate (**11**) was prepared as a more soluble salt by cation exchange of **10** with tetrabutylammonium chloride in acetonitrile. Solubility of **10** was indeed improved but the yield of subporphyrin was not improved. In the next step, we focused on the precursor **12** that is sufficiently soluble in common organic solvents and has sufficient stabilities toward moisture and oxygen. Synthesis of *meso*-aryl-substituted subporphyrins was attempted by the reaction of **12** with aryl aldehydes in CH<sub>2</sub>-Cl<sub>2</sub> under the standard Rothemund–Lindsey conditions. TLC monitoring of the reaction mixture revealed the appearance of several new spots along with consumption of the aryl aldehyde, but subsequent oxidation of this reaction mixture with DDQ or *p*-chloranil did not yield subporphyrin **13**. We thus examined the Adler porphyrin synthesis conditions with chloroacetic acid in toluene, which yielded subporphyrin **13** in low but reproduc-

ible yields (<1%). In the meanwhile, we found that the reaction solvent has a significant influence on the yield of subporphyrin under the Adler conditions; high boiling solvents such as *p*-xylene, mesitylene, and 1,2-dichlorobenzene achieved better yields with increase of boiling points, whereas the yields of subporphyrin were decreased slightly in refluxing 1,2,4-trichlorobenzene or diphenyl ether of which boiling points are higher than 180 °C. On the basis of these results, we employed 1,2-dichlorobenzene as the optimal solvent for detailed examination of the subporphyrin synthesis. In the course of optimization, we noted that a serious bothersome side reaction was the acid-promoted scrambling of **12**, which liberated pyrrole gradually. In fact, a substantial amount of tetraarylporphyrin was formed in every run. To make the situation worse, such liberated pyrrole consumed both **12** and the aryl aldehyde, possibly through condensation. We thus added an excess amount of the aryl aldehyde (9 equiv to **12**), which actually suppressed the formation of porphyrinic and polymeric byproducts. Under such conditions, subporphyrins were isolated as their B-methoxy forms, **14a**, **14b**, **14c**, **14d**, **14e**, and **14f** in 2.3, 2.0, 2.2, 3.2, 2.3, and 1.5% yields, respectively (Scheme 1). In case of **13g** bearing *ortho*, *ortho*-dimethoxy-substituted phenyl groups, the reaction was rather sluggish to provide **14g** only in 1.1% yield.

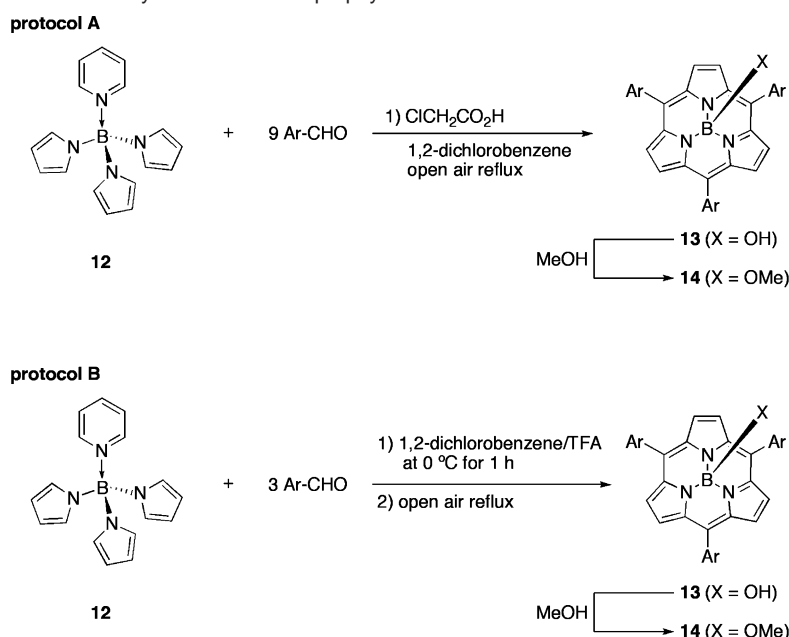
The introduction of an adequate axial substituent to the center boron is essential for the successful isolation of products, as well as special cares during chromatographic separation. Previously, we reported that B-methoxy isomer was the most stable for tribenzosubporphines **7**. The same trend was found also valid for this series, and *meso*-aryl-substituted subporphyrins were also isolated as their B-methoxy form, **14**. In our synthetic procedure, subporphyrins were formed mainly as B-hydroxo forms **13** via coordination of water formed during the condensation of **12** and aldehyde, but were easily converted to their B-methoxy forms **14** quantitatively upon refluxing in methanol. Under the similar conditions, B-alkoxo subporphyrins could be also prepared, but B-methoxy subporphyrins **14** were found to be the most stable toward hydrolytic cleavage. This feature prompted us to isolate subporphyrins as their B-methoxy forms **14**. In addition, we found that the separation of subporphyrins **13** from the reaction mixtures needed particular care. The most troublesome impurities at the separation step were tailing polymeric byproducts that occluded subporphyrins, retaining them on silica gel. Once the reaction mixture was evaporated to dryness, the elution of subporphyrins **13** over a silica gel column become quite difficult, which precluded its isolation. This feature is in sharp contrast to the observation that, once purified, subporphyrins **13** and **14** elute rather smoothly without any serious adsorbing. It was thus considered that usual chromatography of the crude mixture over a silica gel column resulted in serious loss of **13**. In fact, we found that extraction of **13** from the reaction mixture once adsorbed on silica gel was very tedious, requiring repeated treatments with a mixture of methanol and trifluoroacetic acid (TFA) (20:1). Thus, after the macrocyclization reaction was completed, subporphyrins **14** were isolated as follows: (1) the axial ligand was changed to methoxy group by heating in a mixture of THF and methanol, (2) the polymeric materials were removed by size exclusion column chromatography to obtain roughly purified subporphyrin as a yellowish brown fraction, (3) the crude subporphyrin was

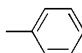
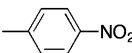
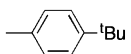
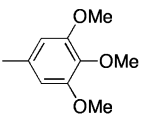
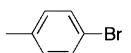
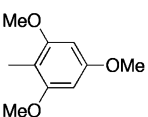
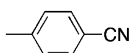
(17) Myślubski, R.; Latos-Grażyński, L.; Sztterenber, L.; Lis, T. *Angew. Chem., Int. Ed.* **2006**, *45*, 3670–3674.

(18) Pacholska, E.; Latos-Grażyński, L.; Ciunik, Z. *Chem. Eur. J.* **2002**, *8*, 5403–5406.

(19) (a) Wrackmeyer, B.; Schwarze, B.; Milius, W. *Inorg. Chim. Acta.* **1996**, *241*, 87–93. (b) Douglade, G.; Fabre, B. *Synth. Met.* **2002**, *129*, 309–314.

(20) (a) Köster, R.; Bellut, H.; Hattori, S. *Liebigs Ann. Chem.* **1968**, *720*, 1–22. (b) Szarvas, P.; Györi, B.; Emri, J. *Acta. Chim. (Budapest)* **1971**, *70*, 1–8.

**Scheme 1.** Synthesis of *meso*-Aryl-Substituted Subporphyrins

	-Ar =	yield (%)			-Ar =	yield (%)	
		protocol A	protocol B			protocol A	protocol B
<b>14a</b>		2.3	3.8	<b>14e</b>		2.3	2.8
<b>14b</b>		2.0	5.6	<b>14f</b>		1.5	5.6
<b>14c</b>		2.2	4.3	<b>14g</b>		1.1	trace
<b>14d</b>		3.2	3.5				

further purified by silica gel column chromatography, (4) the almost pure subporphyrin was again completely converted to its B-methoxy form **14**, and (5) final recrystallization from its methanol solution gave pure **14** as orange solids. In separation by column chromatography, it is important to check each fraction by monitoring green fluorescence of **14**.

In an alternative protocol, we examined a one-pot two-step reaction under milder conditions, in which **12** and an aryl aldehyde were condensed in the presence of TFA at 0 °C under inert atmosphere for 1 h in order to avoid acid-promoted scrambling. After being quenched with pyridine, the reaction mixture was refluxed in *o*-dichlorobenzene for 1 h to complete air oxidation. This method provided pure subporphyrins **14a**, **14b**, **14c**, **14d**, **14e**, and **14f** in 3.8, 5.6, 4.3, 3.5, 2.8, and 5.6% yields, respectively, after the separation and isolation procedures described above. This protocol gave better yields for sterically unhindered aryl aldehydes. However, the subporphyrin **14g** was not obtained by this method, although its formation was confirmed by TLC and MALDI-TOF mass analysis of the

reaction mixture. Following the second protocol and the standard isolation procedures, we prepared **14c** in a large scale (~300 mg) in one-batch synthesis.

**Characterization: Mass and NMR Measurements.** High-resolution electrospray ionization (HR-ESI) mass spectra of subporphyrins **14** exhibited intense borenium cation peaks [**14**-OMe]<sup>+</sup> which were generated as a consequence of elimination of the axial methoxy group. For example, **14b**, **14d**, and **14g** showed the parent cation signals at *m/z* = 638.3693, 545.1683, and 740.2787 which correspond to [**14b**-OMe]<sup>+</sup> (calcd for [C<sub>45</sub>H<sub>45</sub>N<sub>3</sub>B<sub>1</sub>]<sup>+</sup>: *m/z* 638.3709), [**14d** - OMe]<sup>+</sup> (calcd for [C<sub>36</sub>H<sub>18</sub>N<sub>6</sub>B<sub>1</sub>]<sup>+</sup>: *m/z* 545.1687), and [**14g** - OMe]<sup>+</sup> (calcd for [C<sub>42</sub>H<sub>39</sub>N<sub>3</sub>O<sub>9</sub>B<sub>1</sub>]<sup>+</sup>: *m/z* 740.2781), respectively. In our measurement conditions, the ion peaks of [**14**]<sup>+</sup> were too weak to be observed compared with those of the borenium cations. Among the series, **14f** gave slightly intense and observable cation peak at *m/z* = 771.2970 ([**14f**]<sup>+</sup>, calcd for [C<sub>43</sub>H<sub>42</sub>N<sub>3</sub>O<sub>10</sub>B<sub>1</sub>]<sup>+</sup>: *m/z* 771.2965); however, its intensity was less than 1% that of borenium peak [**14f** - OMe]<sup>+</sup>, although, methoxo(tribenzosub-

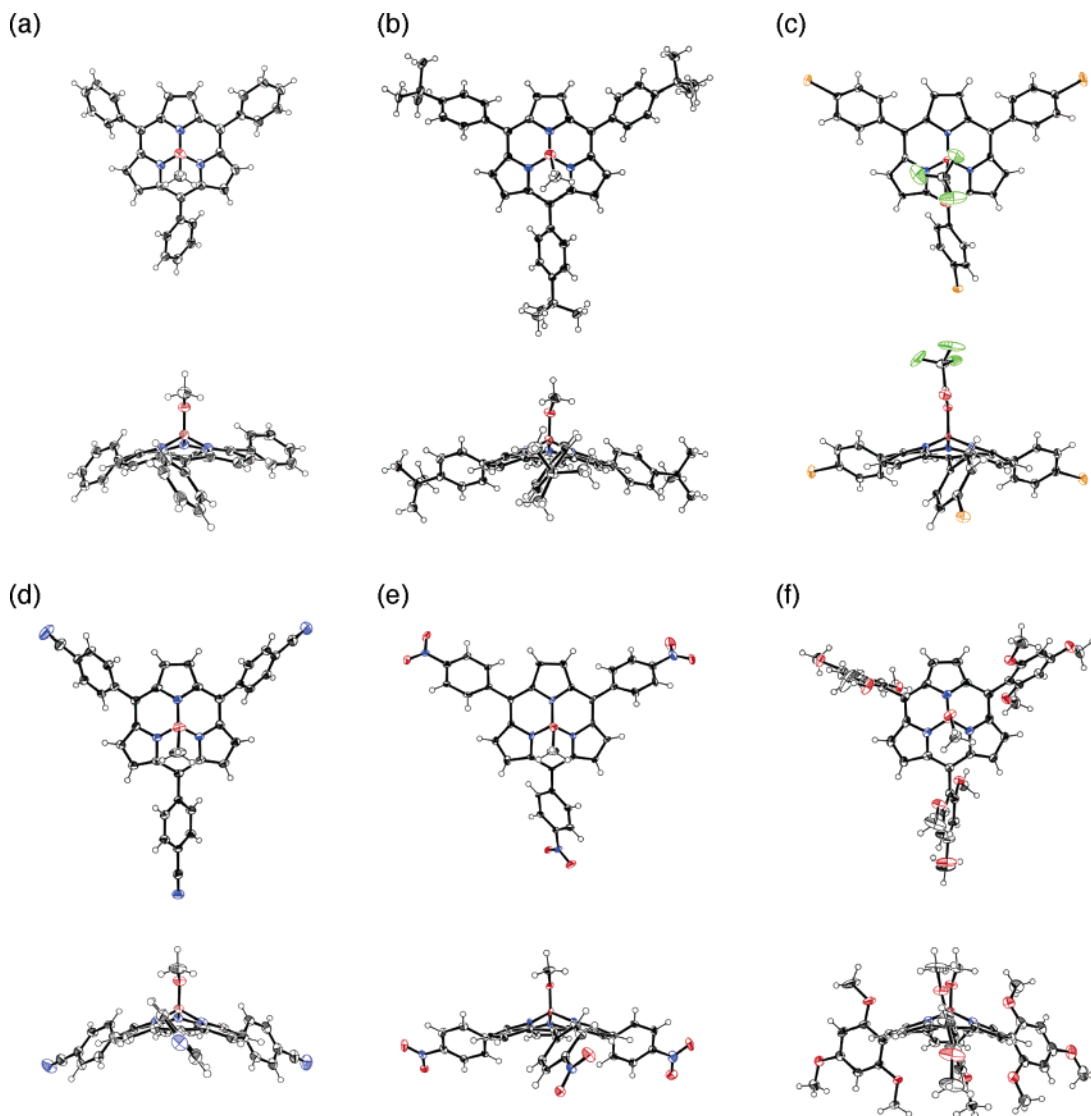


**Figure 1.** Crystal structures of (a) **14a**, (b) **14b**, (c) **15c**, (d) **14d**, (e) **14e**, and (f) **14g** at 50% probability of thermal ellipsoids (boron: brown, carbon: black, nitrogen: blue, oxygen: red, fluorine: yellow-green, and bromine: orange). Solvent molecules are omitted for clarity.

porphinato)boron **7-OMe** ( $X = \text{OMe}$ ) displays these two types of cation peaks in  $\sim 10:3$  (borenium/methoxy-coordinated) ratio under the same settings.<sup>21</sup>

The  $^1\text{H}$  NMR spectrum of **14a** in  $\text{CDCl}_3$  is very simple, exhibiting a singlet at 8.12 ppm due to the peripheral  $\beta$ -protons in line with its  $C_3$ -symmetric structure. Importantly, the protons of the *meso*-phenyl substituents are observed as a single set of three signals at 8.06 (*ortho*, doublet,  $J = 7.8$  Hz, 6H), 7.60 (*meta*, pseudotriplet,  $J = 7.5$  Hz, 6H), and 7.61 ppm (*para*, triplet,  $J = 7.3$  Hz, 3H), suggesting free rotation of these phenyl groups, considering its conelike bent structure. Subporphyrins **14b–14f** exhibit  $^1\text{H}$  NMR spectra similar to that of **14a** with respect to  $C_3$ -symmetric structure and free rotation of the *meso*-aryl substituents. On the other hand, 2,4,6-trimethoxyphenyl-substituted subporphyrin **14g** exhibits a remarkably shielded  $\beta$ -proton signal at 7.63 ppm as a consequence of very effective shielding influence of the neighboring *meso*-aryl substituents. Restricted rotation of the *meso*-2,4,6-trimethoxyphenyl substituents is clearly indicated by different chemical shifts of the 3-

and 5-protons observed at 6.50 and 6.32 ppm, which in turn, suggest their rather perpendicular orientation with respect to the subporphyrin macrocycle.

Characteristic high-field shifts of the axial methoxy group of **14** that are observed at 0.95–0.79 ppm are also important, since they indicate the diatropic ring current arising from  $14\pi$  aromatic macrocycles. We also found that the chemical shifts of the central boron atom in the  $^{11}\text{B}$  NMR spectra would help evaluate the aromatic character of subporphyrins, which are characteristically observed in a shielded range of  $-15.2$  to  $-15.4$  ppm as broad signals in  $\text{CDCl}_3$ .

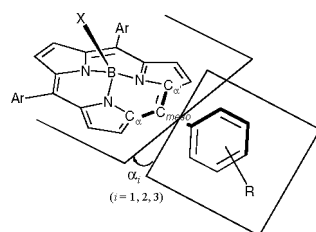
**X-ray Diffraction Analysis.** Single crystals of **14a**, **14b**, **14d**, **14e**, and **14g** suitable for X-ray diffraction analysis were obtained from slow recrystallization from their methanol solutions, while single crystals of trifluoroacetate coordinated subporphyrin, **15c** ( $X = \text{OCOCF}_3$ ) were obtained from slow vapor diffusion of a dichloromethane solution of **14c** in the presence of trifluoroacetic acid (Figure 1 and Table 1). The crystal structures thus determined revealed the bowl-like triangular shapes with variable curvatures that depend upon axial ligands and crystal-packing manners, similar to those of

(21) Inokuma, Y.; Kwon, J. H.; Ahn, T. K.; Yoon, M. C.; Kim, D.; Osuka, A. *Angew. Chem., Int. Ed.* **2006**, *45*, 961–964.

**Table 1.** Selected Bond Lengths and Angles, and Bowl-depths of Subporphyrins

compd	N–B (Å)	B–O (Å)	$\alpha_i^a$ (deg)	bowl-depth <sup>b</sup> (Å)	compd	N–B (Å)	B–O (Å)	$\alpha_i^a$ (deg)	bowl-depth <sup>b</sup> (Å)
<b>14a<sup>c</sup></b>	1.485(4)	1.438(4)	38.3	1.29	<b>14d</b>	1.485(4)	1.440(4)	45.8	1.40
	1.500(4)		45.7			1.496(5)		50.9	
	1.507(4)		48.1			1.509(4)		55.7	
<b>14b</b>	1.493(3)	1.451(3)	43.5	1.35	<b>14e<sup>c</sup></b>	1.483(8)	1.442(8)	42.3	1.29
	1.495(3)		45.9			1.490(8)		47.8	
	1.500(3)		52.1			1.512(7)		51.3	
<b>15c</b>	1.470(5)	1.519(5)	44.2	1.30	<b>14g</b>	1.495(4)	1.448(3)	68.7	1.44
	1.471(5)		46.5			1.495(4)		71.8	
	1.480(5)		54.6			1.495(4)		75.7	

<sup>a</sup> Angles  $\alpha_i$  ( $i = 1, 2, 3$ ) are defined by the dihedral angle between the plane of  $C_\alpha-C_{meso}-C_\alpha$  and the mean plane of *meso*-phenyl ring.



<sup>b</sup> Bowl-depth is defined by the distance from the boron atom to the mean plane of peripheral six  $\beta$ -carbons. <sup>c</sup> Data are of one representative molecule in the unit lattice.

tribenzosubporphyrins **7**. The degree of curvatures can be characterized by the bowl-depth defined by the distance from the mean plane of peripheral six  $\beta$ -carbons to the center boron atom. In this definition, the tribenzosubporphyrins **7** possess bowl-depths in the range of 1.18–1.41 Å. In this series, bowl-depths of subporphyrin **14** and **15c** vary in the range of 1.29–1.44 Å depending on the *meso*-aryl groups and axial substituents. The bond distance of B–O in **15c** slightly longer than those in other methoxo derivatives is notable, since it suggests contribution of ionic binding character of the trifluoroacetate ligand. Three B–N bonds in subporphyrins **14** and **15c** shown in Table 1 are slightly shorter than **7** (N–B distance 1.50–1.51 Å for alkoxo-form), and such a difference was also observed for zinc complexes of porphyrins and their tetrabenzoporphyrin analogues<sup>22</sup> (Zn–N bond lengths are 2.04 Å for ZnTPP and 2.08 Å for ZnTBP<sup>23</sup>). These observations may be attributed to the increased donating character of the pyrrolic nitrogen in **14**, due to the absence of electron-withdrawing fused benzene rings in peripheral positions.

Another important structural characteristics are relatively small dihedral angles of *meso*-substituted aryl groups in subporphyrins **14a–e** that range only in 38.3–55.7°, while the 2,4,6-trimethoxyphenyl groups in **14g** show larger dihedral angles (68.7–75.7°) due to the steric hindrance of the *ortho*-methoxy substituents. These features are in contrast to those of 5,10,15,20-tetraarylporphyrins, which usually exhibit larger dihedral angles (>60°), and even larger values (78–82°)<sup>24</sup> for those bearing 2,4,6-trimethoxy-substituted aryl groups. The observed small dihedral angles of the *meso*-aryl substituents, which are understandable in terms of their small angles of  $C_\alpha-C_{meso}-C_\alpha'$  give rise to stronger electronic influences of the *meso*-aryl substituents on the electronic properties of the subporphyrins. This will be discussed in detail below.

**Rotation of *meso*-Aryl Groups.** Rotation of phenyl rings at *meso* positions is of particular importance for understanding the structural and electronic properties of subporphyrins. As the X-ray diffraction and <sup>1</sup>H NMR analyses indicated, subporphyrins **14** have more rotational freedom and thus lower rotational barriers for *meso*-aryl substituents in comparison to those of porphyrins. Rotation of phenyl rings at *meso* positions on porphyrin is restricted due to steric interaction with neighboring  $\beta$ -C–H groups, and the eight protons on the *ortho*-positions of phenyl rings are observed as a couple of doublets at low temperatures ( $\leq 10$  °C) in  $\eta^5$ -coordinated ruthenium carbonyl, indium chloride, and titanyl complexes. In the cases of **14**, their convex and concave faces are nonequivalent and permit the detection of the rotation of *meso*-phenyl groups by <sup>1</sup>H NMR spectroscopy. At room temperature, *para*-substituted subporphyrins **14b** exhibit only two doublets at 7.70 and 8.60 ppm due to the *ortho*- and *meta*-protons, respectively, and 3,4,5-trimethoxyphenyl groups of **14f** exhibit only three sharp singlets at 7.24, 3.96, and 3.95 ppm due to the *ortho*-aromatic protons, *meta*-methoxy protons, and *para*-methoxy protons, respectively, indicating the free rotation of *meso*-aryl substituents. In contrast, 2,4,6-trimethoxyphenyl subporphyrin **14g** shows split *meta*-aromatic proton signals at 6.50 and 6.32 ppm as a pair of doublets with a coupling constant of  $J = 3.2$  Hz and two singlets at 3.79 and 3.32 ppm due to the methoxy protons at 2,6-position, clearly indicating the restricted rotation of the *meso*-aryl groups. The variable-temperature (VT) <sup>1</sup>H NMR method has been used for the temperature dependence of the rotation of the *meso*-aryl substitutions. With decreasing temperature, the <sup>1</sup>H NMR signals of the *meta*-aromatic protons and the methoxy protons of **14f** became gradually broadened with gradual high-field shifts but did not split into two signals even at –90 °C (Figure 2), indicating the coalescence temperature should be lower than –90 °C. On the other hand, with increasing temperature, the split signals of the *ortho*-aromatic protons and *meta*-methoxy protons of **14g** became significantly broadened with slight low-field shifts but did not merge to single signals at 130 °C, indicating that the coalescence temperature should be even

(22) In *adj*-dibenzoporphyrin moiety,  $N_{pyrrolic}-Zn$  and  $N_{isoindolic}-Zn$  distances are 2.06 and 2.09 Å, respectively. Inokuma, Y.; Ono, N.; Uno, H.; Kim, D. Y.; Noh, S. B.; Kim, D.; Osuka, A. *Chem. Commun.* **2005**, 3782–3784.

(23) Cheng, R. J.; Chen, Y. R.; Wang, S. L.; Cheng, C. Y. *Polyhedron* **1993**, *12*, 1353–1360.

(24) Gold, K. W.; Hodgson, D. J.; Gold, A.; Savrin, J. E.; Toney, G. E. *J. Chem. Soc., Chem. Commun.* **1985**, 563–564.

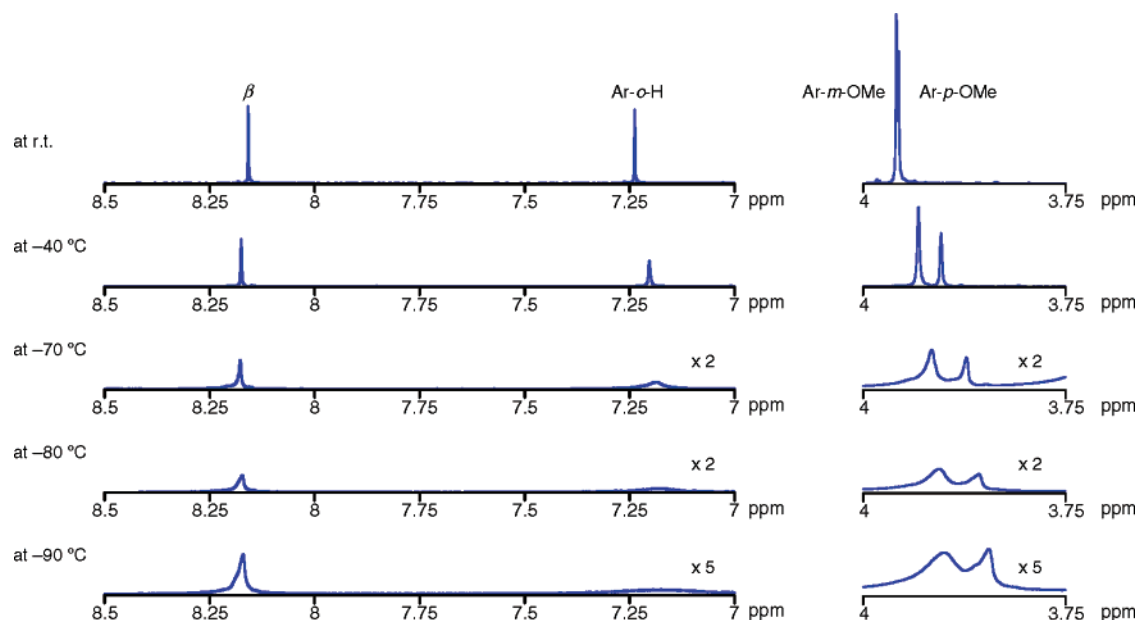


**Figure 2.**  $^1\text{H}$  NMR spectra of subporphyrin **14f** in  $\text{CD}_2\text{Cl}_2$  containing 1% (v/v) of MeOH at room temperature,  $-40$ ,  $-70$ ,  $-80$ , and  $-90$   $^\circ\text{C}$ .

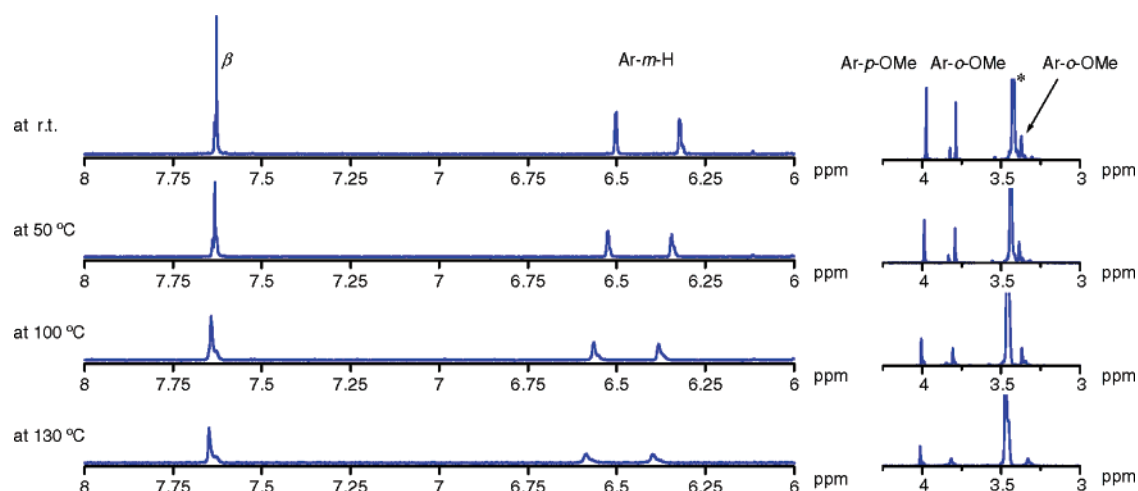


**Figure 3.**  $^1\text{H}$  NMR spectra of subporphyrin **14g** in tetrachloroethane- $d_2$  at room temperature,  $50$ ,  $100$ , and  $130$   $^\circ\text{C}$ .

**Table 2.** Oxidation and Reduction Potentials of Subporphyrin **14a–g** in Acetonitrile (in V vs Ferrocene/Ferrocenium Ion Pair)<sup>a</sup>

compd	oxidation		reduction			HOMO–LUMO gap (eV)
	$E_{1/2,ox}^1$	$E_{1/2,ox}^2$	$E_{1/2,red}^1$	$E_{1/2,red}^2$	$E_{1/2,red}^3$	
<b>14a</b>	0.78		−1.82			2.60
<b>14b</b>	0.72		−1.83			2.55
<b>14c</b>	0.84		−1.70			2.54
<b>14d</b>	1.02		−1.53	−1.73	−1.90	2.55
<b>14e</b>	1.00		−1.30 <sup>b</sup>			2.30
<b>14f</b>	0.64		−1.80			2.44
<b>14g</b>	0.65	0.88	−2.10			2.75

<sup>a</sup> These values were measured by cyclic voltammetry using a glassy carbon or platinum working electrode, a platinum wire counter electrode, and  $\text{Ag}/0.01\text{ M AgClO}_4$  reference electrode. The measurements were carried out in acetonitrile solutions containing  $0.10\text{ M Bu}_4\text{NPF}_6$  as a supporting electrolyte. <sup>b</sup> Multi-electron reduction.

higher (Figure 3). These VT-NMR measurements suggest a much smaller rotational barrier of *ortho*-nonsubstituted phenyl rings in subporphyrin **14** than that in porphyrins, and that their rotation can be controlled by steric hindrance of *ortho*-methoxy groups in a wide temperature range. Furthermore, these results

are in accordance with the observed low tilting angles of *meso*-aryl groups in **14b**, **15c**, **14d**, and **14e**, and highly twisted manner of **14g** in their crystal structures.

**Electrochemistry and MO Calculations.** The oxidation and reduction potentials of **14** have been measured by cyclic voltammetry to examine the influence of *meso*-aryl substituents on the electronic  $\pi$ -system of subporphyrins (Table 2). For **14a–f**, the first one-electron oxidations were observed as reversible waves in the range of  $0.64$ – $1.02\text{ V}$  versus the ferrocene/ferrocenium ion couple, but the second oxidation steps were irreversible. On the other hand, the first and second oxidation waves of **14g** were both reversible at  $0.65$  and  $0.88\text{ V}$ . Importantly, a plot of the first oxidation potentials of **14a–e** versus the Hammett  $\sigma$  values constitutes a nice straight line (Figure 4).

The first reduction potentials of **14a–c**, **14f**, and **14g** were also observed as reversible waves in the range of  $-1.7$  to  $-2.1\text{ V}$  (Table 2). Subporphyrins **14d** and **14e**, which have strong electron-withdrawing substituents at the *para*-positions, exhibited different multireduction processes. 4-Cyanophenyl-substituted subporphyrin **14d** displayed three reversible reduction

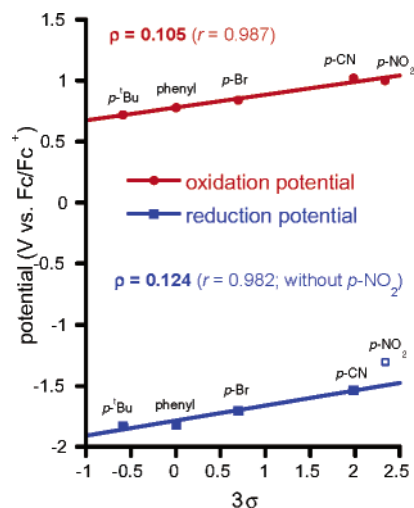


**Figure 4.** Plot of oxidation (red) and reduction (blue) potentials vs Hammett- $3\sigma$  values of *para* substituents on subporphyrin **14a–e**.

waves at  $-1.53$ ,  $-1.73$ , and  $-1.90$  V all as single-electron reduction processes, and 4-nitrophenyl-substituted subporphyrin **14e** showed a much larger reduction wave at  $-1.30$  V. On the basis of the ratio  $I_{p,ox}/I_{p,red}$ , which is proportional to  $(n_{ox}/n_{red})^{3/2}$ , the number of electrons concerned with the first reduction process of **14e** has been estimated to be three ( $n_{ox}/n_{red} = 1/2.80$ ; From the DPV result in which  $I_p \propto n^2$ ,  $n_{ox}/n_{red}$  is also determined to be  $1/2.79$ ). A plot of the first reduction potentials versus the Hammett  $\sigma$  values also constitutes a nice straight line for **14a–d** except for **14e**. This result suggests that the first reductions of **14a–d** took place at the subporphyrin  $\pi$ -system (LUMO orbital of the subporphyrin) but that of **14e** might occur at different sites, probably at the *meso*-substituted 4-nitrophenyl groups.

MO calculations were performed at the B3LYP/6-31G\* level with the Gaussian03 package.<sup>25</sup> We first compared the molecular orbitals of **14b** and **14g** to examine the influence of free rotation of *meso*-aryl substituents. As shown in Figure 5, both **14b** and **14g** possess quite porphyrin-like four orbitals, HOMO-1, HOMO, LUMO, and LUMO+1. The HOMO and HOMO-1 of **14b** and **14g** closely resemble the  $a_{2u}$  (HOMO) and  $a_{1u}$  (HOMO-1) orbitals of *meso*-tetraphenylporphyrin (TPP), despite their pseudo  $C_3$ -symmetry, and the LUMO and LUMO+1 are similar to those of porphyrin  $e_g$  orbitals. Next, we examined the molecular orbitals of **14d**. While the HOMOs of **14d** are quite similar to those of **14b** and **14g**, calculated LUMO to LUMO+4 of **14d** suggest slight but notable interactions of LUMOs of the subporphyrin and *meso*-(4-cyanophenyl) moieties. These interactions may be facilitated by relatively low LUMO of *meso*-(4-cyanophenyl) substituents that can interact with relatively high LUMO level of  $14\pi$ -subporphyrin. Characteristically, the lowest three unoccupied orbitals, LUMO, LUMO+1, and LUMO+2, of **14e** are dominated by *meso*-(4-nitrophenyl) groups, and the core-related orbitals are higher in energy as LUMO+3 and LUMO+4, although these orbitals are located in 0.8 V range. Namely, the LUMO of **14e** is mainly lying at the electron-deficient *meso*-(4-nitrophenyl) groups and not the subporphyrin core. In addition, small energy differences among these molecular orbitals lead to effective hybridization of five unoccupied orbitals.

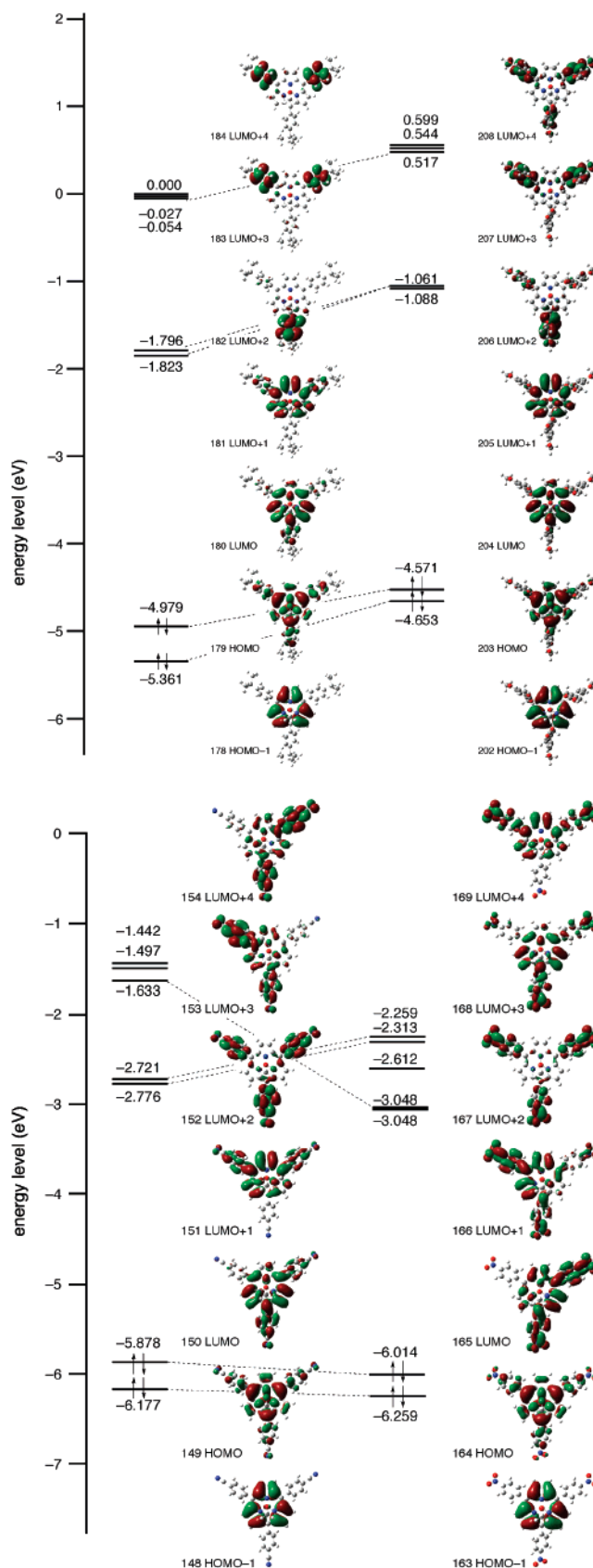


**Figure 5.** Selected molecular orbitals for **14d** (top, left) and **14g** (top, right), **14d** (bottom, left), and **14e** (bottom, right) calculated at the B3LYP/6-31G\* level.

(25) (a) Frisch, M. J.; et al. *Gaussian 03*, Revision B.05; Gaussian, Inc.: Pittsburgh, PA, 2003. (b) Becke, A. D. *Phys. Rev. A* **1988**, *38*, 3098–3100. (c) Lee, C.; Yang, W.; Parr, R. G. *Phys. Rev. B* **1988**, *37*, 785–789.

As applied for *para*-substituted tetraphenylporphyrins,  $E_{1/2}$  potentials of *para*-substituted subporphyrin **14a–e** obtained by



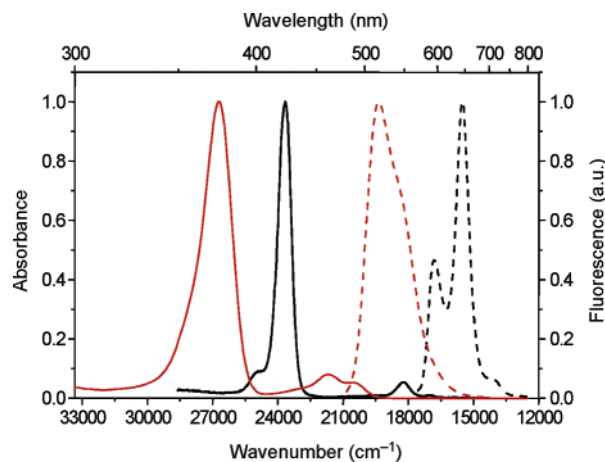


**Figure 6.** Steady-state absorption (solid lines) and fluorescence (dashed lines) spectra of ZnTPP (black) and **14a** (red) in toluene.

cyclic voltammetry are plotted as a function of Hammett's parameter.<sup>26</sup> Since these subporphyrins have three substituents on each of *meso*-phenyl rings,  $3\sigma$  is used as the total substituent constant, and the reaction constant  $\rho$  was calculated by following equation:

$$\Delta E_{1/2} = 3\sigma\rho$$

The plot of the oxidation potentials  $E_{1/2}$  vs  $3\sigma$ , when analyzed by least-squares method, gave a good linear correlation of a slope,  $\rho = 0.105$  V, with a correlation coefficient of  $r = 0.987$  (Figure 4). This slope is quite large as compared with the reported value of corresponding TPP ( $\rho = 0.065$  V in the plot of  $E_{1/2}$  vs  $4\sigma$ ). The similar plot of the reduction potentials  $E_{1/2}$  shows that the value of **14e** lies out of linear correlation. Thus, the least-square analysis of the rest of the data provided a slope  $\rho = 0.124$  V with  $r = 0.982$ , which is also larger than the reported value of the corresponding TPP ( $\rho = 0.073$  V in the plot of  $E_{1/2}$  vs  $4\sigma$ ). Judging from these results and the MO calculations, the first reduction of **14e** has been considered to occur at the *meso*-nitrophenyl groups. Furthermore, the higher reduction level of **14e**,  $E_{1/2} = -1.30$  V (vs Fc/Fc<sup>+</sup>), than the reported reduction potential of nitrobenzene ( $E_{1/2} = -1.6$  V)<sup>27</sup> may arise from orbital stabilization due to the interactions with the subporphyrin.

**Optical Properties. Steady-State Absorption and Emission Spectra.** Figure 6 shows the steady-state absorption and fluorescence spectra of subporphyrin **14a** and ZnTPP in toluene. A blue-shifted and broader spectrum was observed for **14a** as compared to that of ZnTPP. The blue-shift in **14a** is considered to originate from the reduced number of  $\pi$ -electrons ( $14\pi$  for subporphyrin and  $18\pi$  for ZnTPP) participating in their  $\pi$ -conjugation pathways. The smeared vibronic structure in Q-like absorption and broad fluorescence bands seems to arise from the bowl-shaped subporphyrin core in contrast to the comparatively flat structure of ZnTPP.

As indicated above, the electronic properties of subporphyrins are largely influenced by *meso*-aryl substituents due to their

flexible rotation. Examination of the absorption and fluorescence spectra led to classification into three groups (Figure 7 and Table 3). The first group includes **14a**, **14b**, **14c**, **14d**, and **14f**, which bear freely rotatable *meso*-aryl substituents. Figure 7a shows the absorption and fluorescence spectra of **14b** as the representative example. The absorption spectrum shows an intense Soret-band at 377 nm and two relatively weak Q-bands at 465 and 491 nm. The fluorescence emission of **14b** was observed as a mirror image of the Q-band at 524 nm with the fluorescence quantum yield ( $\Phi_F$ ) of 0.16 in CH<sub>2</sub>Cl<sub>2</sub>. Other subporphyrins (**14a**, **14c**, and **14d**) in this group exhibit similar optical properties as summarized in Table 3. (4-Bromophenyl)subporphyrin **14c** exhibits considerably reduced fluorescence quantum yield ( $\Phi_F = 8 \times 10^{-3}$ ) presumably due to the intramolecular heavy-atom effect that enhances the intersystem crossing to the triplet excited state. This effect is known for tetrakis(4-bromophenyl)porphyrin<sup>28</sup> but is stronger in the subporphyrin **14c**, as evidenced from the fluorescence quenching in **14a** (94% stronger than that of tetra(4-bromophenyl)porphyrin (87%).

The subporphyrin **14g** bearing hindered 2,4,6-trimethoxyphenyl *meso* substituents exhibits optical properties that are different from those of the first group and thus was grouped into the second group (Figure 7b). The subporphyrin **14g** exhibits a Soret band at 372 nm and only one band at 454 nm in the Q-band region, and its fluorescence was observed at 524 nm with a shoulder at 500 nm as a narrower band (475–600 nm) as compared with those in the first group (500–700 nm). The fluorescence quantum yield of **14g** was determined to be 0.11, which was comparable to those of the subporphyrins in the first group.

As the third group, 4-nitrophenyl-substituted subporphyrin **14e** exhibits unique optical properties. Characteristically, during the separation and purification steps, the green fluorescence of **14e** was found to be quenched strongly on silica gel, and its crystalline solids exhibit a distinctive reddish color. Figure 7c shows its absorption and fluorescence spectra, in which the Soret-band is broad and bathochromically shifted to near visible region (~400 nm) and its molar extinction coefficient of  $\epsilon = 1.1 \times 10^5$  M<sup>-1</sup> cm<sup>-1</sup> is significantly lower than those of the others. In addition, **14e** exhibited solvatochromic absorption changes, which shifted the Soret-band in the range of 389–399 nm, and the relative intensities of two Q-bands at 470 and 490 nm were sensitively changed in response to solvents. Although its fluorescence emission behavior in CH<sub>2</sub>Cl<sub>2</sub> is quite similar to that of the general type (Figure 7a), the fluorescence quantum yield was progressively reduced with increasing solvent polarity:  $\Phi_F = 0.194$  in toluene, 0.183 in ethyl acetate, 0.154 in dichloromethane, 0.112 in *N,N*-dimethylformamide, 0.010 in acetonitrile, and 0.002 in methanol (Figure 7c and SI). These phenomena, which have not been observed for other subporphyrins, are similar to those of peripherally nitrated porphyrins.<sup>29</sup> A possible explanation is that the singlet excited state of **14e** has intramolecular charge-transfer character of [(subporphyrin<sup>δ+</sup>)-(NO<sub>2</sub><sup>δ-</sup>)], which has been supported by MO calculations. Such

(28) Quimby, D. J.; Longo, F. R. *J. Am. Chem. Soc.* **1975**, *97*, 5111–5117.

(26) Substituent constants were of reported values by McDaniel and Brown. McDaniel, D. H.; Brown, H. C. *J. Org. Chem.* **1958**, *23*, 420–427.

(27) (a) Bu, J.; Lilienthal, Woods, J. E.; Nohrden, C. E.; Hoang, K. T.; Truong, D.; Smith, D. K. (b) Bento, M. F.; Medeiros, M. J.; Montenegro, M. I.; Beriot, C.; Pletcher, D. *J. Electroanal. Chem.* **1993**, *345*, 273–286.

(29) (a) Gust, D.; Moore, T. A.; Luttrull, D. K.; Seely, G. R.; Bittersmann, E.; Bensasson, R. V.; Rougee, M.; Land, E. J.; Schryver, F. C. D.; Auweraer, M. V. *Photochem. Photobiol.* **1990**, *51*, 419–426. (b) Chirvony, V. S.; Hoek, A.; Schaafsma, T. J.; Pershukovich, P. P.; Filatov, I. V.; Avilov, I. V.; Shishporenok, S. I.; Terekhov, S. N.; Malinovskii, V. L. *J. Phys. Chem. B* **1998**, *102*, 9714–9724. (c) Takahashi, K.; Hase, S.; Komura, T.; Imanaga, H.; Ohno, O. *Bull. Chem. Soc. Jpn.* **1992**, *65*, 1475–1481.

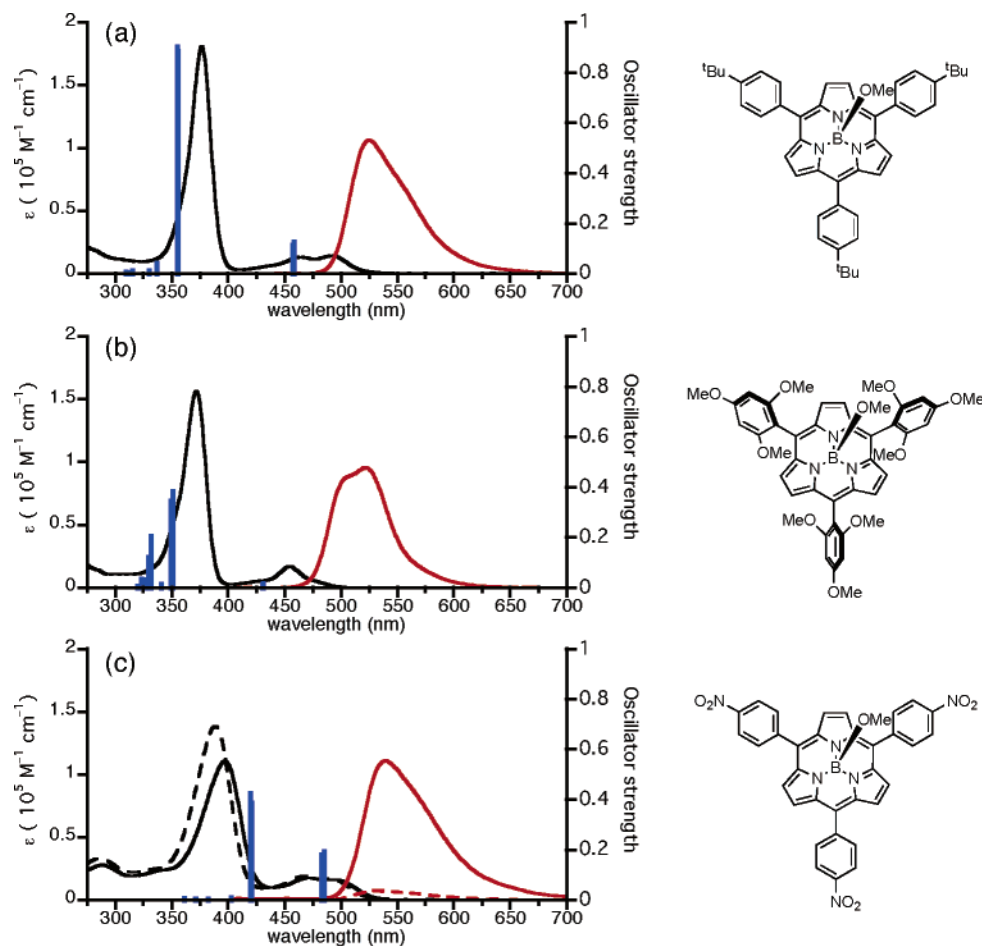


**Figure 7.** UV-vis absorption (black) and fluorescence (red) spectra in dichloromethane (solid line) or methanol (dashed line), and calculated transition (blue bar) by TD-DFT method at the B3LYP/6-31G\* level of (a) **14b**, (b) **14e**, and (c) **14g**.

**Table 3.** Absorption and Fluorescence<sup>a</sup> Data of Subporphyrin **14** in CH<sub>2</sub>Cl<sub>2</sub>

	<b>14a</b>	<b>14b</b>	<b>14c</b>	<b>14d</b>	<b>14e</b>	<b>14f</b>	<b>14g</b>
absorption maxima (nm)	373 (16.6)	377 (18.2)	375 (17.0)	380 (19.2)	397 (11.0)	380 (17.6)	372 (15.6)
$\epsilon$ ( $10^4 \text{ M}^{-1} \text{ cm}^{-1}$ )	461 (1.3)	465 (1.3)	461 (1.3)	465 (1.7)	471 (1.8)	464 (1.3)	454 (1.7)
	484 (0.9)	491 (1.4)	487 (1.1)	491 (sh) <sup>b</sup>	492 (1.6)	493 (1.5)	
fluorescence maximum (nm)	516	524	521	522	543	538	524
fluorescence quantum yield	0.14	0.16	0.008	0.17	0.15	0.12	0.11

<sup>a</sup> Subporphyrins were excited at each absorption maxima (372–397 nm). <sup>b</sup> Shoulder peak.

strong substituent effects of *meso*-aryl groups are characteristic of subporphyrins, since the *meso*-aryl substituents are forced to take more perpendicular conformations in porphyrins, which mitigates the effective conjugative interactions. The rotational freedom of *meso*-aryl rings allows strong conjugative electronic interactions with the subporphyrin core. This means that the  $\pi$ -electronic system of subporphyrins can be drastically tunable by judicious choice of *meso*-aryl substituents as an entirely new and promising attribute of the porphyrinic macrocycles.

**2. Fluorescence Excitation Anisotropy.** In order to obtain information on the relative orientation between the absorption and emission transition dipole moments, we measured the fluorescence excitation anisotropy spectra of subporphyrins in mixed solvents with high viscosity paraffin oil (1:99 in

volume)<sup>30</sup> to avoid the anisotropy loss by rotational diffusion motion. The anisotropy value can be given by eq 1,<sup>31</sup>

$$r = \frac{I_{VV} - GI_{VH}}{I_{VV} + 2GI_{VH}} \quad (1)$$

where  $I_{VV}$  corresponds to the vertically polarized excitation and vertically polarized emission intensity,  $I_{VH}$  to the vertically polarized excitation and horizontally polarized emission, and the  $G$  factor is  $I_{HV}/I_{HH}$ , and in our experiment, the  $G$  factor was measured to be 1.7 (Figure 8).

(30) Lakowicz, J. R. *Principles of Fluorescence Spectroscopy*; Kluwer Academic/Plenum Publishers: New York, 1999.

(31) Morandeira, A.; Vauthey, E.; Schuway, A.; Gossauer, A. *J. Phys. Chem. A* **2004**, *108*, 5741–5751.

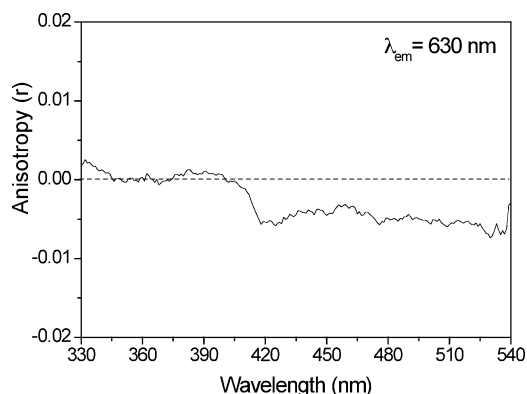


**Figure 8.** Fluorescence excitation anisotropy spectrum of **14a** in toluene (1%) and paraffin oil (99%).

Interestingly, the absolute anisotropy values ( $r$ ) of subporphyrin **14a** were smaller than 0.01 in the whole excitation region, indicating the angle  $\beta$  is close to  $120^\circ$  (or  $60^\circ$ ), reflecting that the reorientation of the transition dipole moment occurs in the triangular geometry of the subporphyrin, according to eq 2,<sup>31</sup>

$$r = \frac{2}{5} \left( \frac{3 \cos^2 \beta - 1}{2} \right) \quad (2)$$

where  $\beta$  is the angle between absorption and fluorescence dipoles. Thus, this result is similar to that of ZnTPP, where the small anisotropy values are interpreted by two perpendicular and degenerate transition dipoles.<sup>30</sup>

**3. Lippert–Mataga Plot Analysis.** The solvent-polarity-dependent spectral changes were analyzed by a Lippert–Mataga plot using eq 3, where the solvent polarity parameter,  $\Delta f$  (orientation polarizability) is a function of the dielectric constant  $\epsilon_r$  and refractive index  $n$  of solvent.<sup>31</sup>

$$\Delta f = \frac{\epsilon_r - 1}{2\epsilon_r + 1} - \frac{n^2 - 1}{2n^2 + 1} \quad (3)$$

Figure 9 shows the Stokes shifts depending on the solvent-polarity parameter. From the slopes of Lippert–Mataga plots as listed in Table 4, the most dynamic change can be found in **14e** as a large positive value (Figure 9a), compared to mild dependence in the other subporphyrins. Thus, the relatively large slope in **14e**, accompanied by the largest variation in fluorescence quantum yields (19–0.2%) depending on solvents, indicates the intramolecular charge-transfer interactions in **14e**.

**4. Fluorescence Lifetime Measurement.** In order to examine the substituent effects on the excited-state dynamics depending on solvents, time-resolved fluorescent decays were measured using a time-correlated single-photon counting method. The decay time constants were obtained by a deconvolution fitting method with instrumental response function (Table 4).<sup>32</sup>

Figure 10 exhibits the representative fluorescence decay profiles of subporphyrins in seven solvents. Figure 10a shows the fluorescence decay profiles of **14g**, which are similar to those of **14a**, **14b**, **14d**, and **14f**, without any critical dependence on solvent polarity. It should be noted that the fluorescence lifetimes of **14g** in seven solvents are longer than those of the other

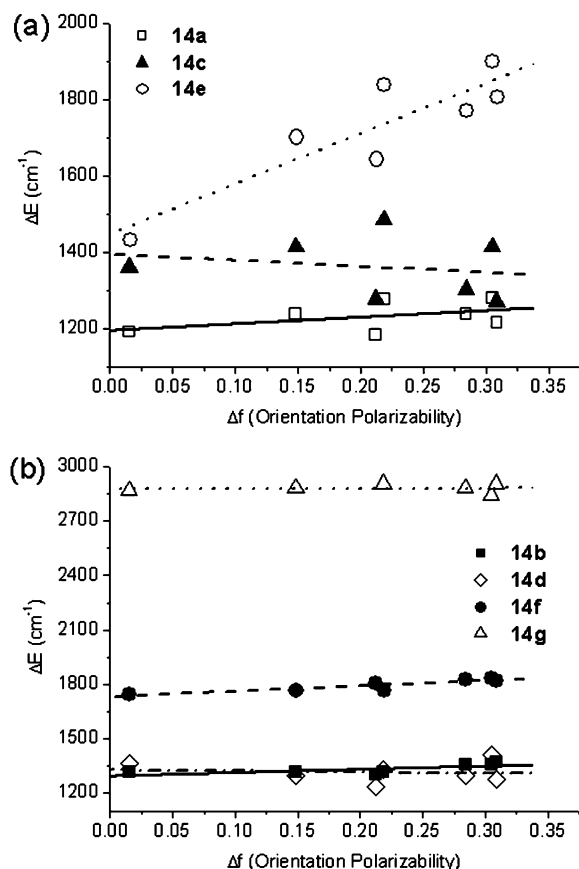


**Figure 9.** Dependence of Stokes shifts ( $\Delta E$ ) on solvent polarity parameter of subporphyrins. (a) **14a**, **14c**, and **14e**. (b) **14b**, **14d**, **14f**, and **14g**. The slopes (in  $\text{cm}^{-1}$ ) of linear fitting are summarized in Table 4.

subporphyrins, which is presumably due to the bulky methoxy groups in the 2,4,6-positions of phenyl rings that prohibit the free rotation of substituent phenyl rings to act as a nonradiative decay channel.

In contrast, in the case of **14e**, there is a strong dependence of fluorescence decay on solvents. In weakly polar solvents, a single-exponential decay was observed with the time constants in the range of 1.98–2.52 ns, which have time constants similar to those in Figure 10a, but in acetonitrile, a very fast decay (0.18 ns) was observed. Moreover, in methanol, the fluorescence decay becomes much faster, close to our instrumental response function. Consistent with the observation in Lippert–Mataga plots, we consider that the photoinduced charge-transfer state plays an important role in the fluorescence-quenching process, occurring from the subporphyrin core to the three *meso*-4-nitrophenyl substituents in **14e**. Especially from the observation of ultrafast fluorescence decay in methanol, it is suggested that hydrogen bonding toward nitrophenyl groups stabilizes the excited state, thus accelerating channel decay via charge transfer. In the previous report,<sup>33</sup> similar charge-transfer behavior was observed in BODIPY (boron–dipyrrin) complexes having two pyrrole rings connected by a methine bridge. In BODIPY, the structural change induced by the rotation of phenylene derivative substituents acts as a driving force of charge transfer.<sup>34</sup>

(32) Ahn, T. K.; Kim, K. S.; Kim, D. Y.; Noh, S. B.; Aratani, N.; Ikeda, C.; Osuka, A.; Kim, D. *J. Am. Chem. Soc.* **2006**, *128*, 1700–1704.

(33) Li, F.; Yang, S. I.; Ciringh, Y.; Seth, J.; Martin, C. H., III; Singh, D. L.; Kim, D.; Birge, R. R.; Bocian, D. F.; Holtz, D.; Lindsey, J. S. *J. Am. Chem. Soc.* **1998**, *120*, 10001–10017.

**Table 4.** Fluorescence Lifetimes (ns), Detection Wavelengths (nm),<sup>a</sup> and the Slope in the Fitting of the Lippert–Mataga Plot (Figure 9)

compd	toluene (nm)	CH <sub>2</sub> Cl <sub>2</sub> (nm)	CHCl <sub>3</sub> (nm)	acetone (nm)	pyridine (nm)	acetonitrile (nm)	MeOH (nm)	slope (cm <sup>-1</sup> )
<b>14a</b>	2.95	2.39	2.45	2.85	2.88	2.88	3.06	171
	(517)	(516)	(516)	(516)	(519)	(516)	(512)	
<b>14b</b>	2.56	2.04	2.06	2.55	2.51	2.55	2.62	186
	(526)	(526)	(526)	(526)	(529)	(526)	(523)	
<b>14c</b>	0.13 <sup>b</sup>	0.13 <sup>b</sup>	0.13 <sup>b</sup>	0.13 <sup>b</sup>	0.13 <sup>b</sup>	0.13 <sup>b</sup>	0.13 <sup>b</sup>	-158
	(525)	(524)	(523)	(520)	(525)	(523)	(518)	
<b>14d</b>	3.23	2.98	2.99	3.69	3.66	3.38	3.82	-63
	(525)	(522)	(522)	(522)	(526)	(523)	(518)	
<b>14e</b>	2.52	1.98	2.24	2.26	2.40	0.18	<0.05 <sup>c</sup>	1319
	(534)	(542)	(537)	(539)	(546)	(544)	(534)	
<b>14f</b>	2.99	2.47	2.35	2.92	2.80	2.86	2.90	302
	(543)	(539)	(540)	(543)	(546)	(542)	(538)	
<b>14g</b>	4.04	3.55	3.46	3.72	3.36	3.69	3.90	17 <sup>d</sup>
	(522)	(523)	(525)	(521)	(510)	(516)	(519)	

<sup>a</sup> The values in parenthesis are the detection wavelengths which correspond to the maximum wavelengths observed in the steady-state emission spectra.

<sup>b</sup> The time constant of 0.13 ns is an average value, where the fluorescence decay signals could be fitted with biexponential components;  $I(t) = A_1 e^{-t/\tau_1} + A_2 e^{-t/\tau_2}$ , where the first amplitude  $A_1$  was >97% with 0.14 ns, and the second  $A_2$  was <3% with 0.51–0.56 ns time constants. <sup>c</sup> The fluorescence decay profile for **14e** in methanol was close to the instrumental response function of our setup. <sup>d</sup> The Stokes shift of **14g** in pyridine was omitted from the linear fitting.

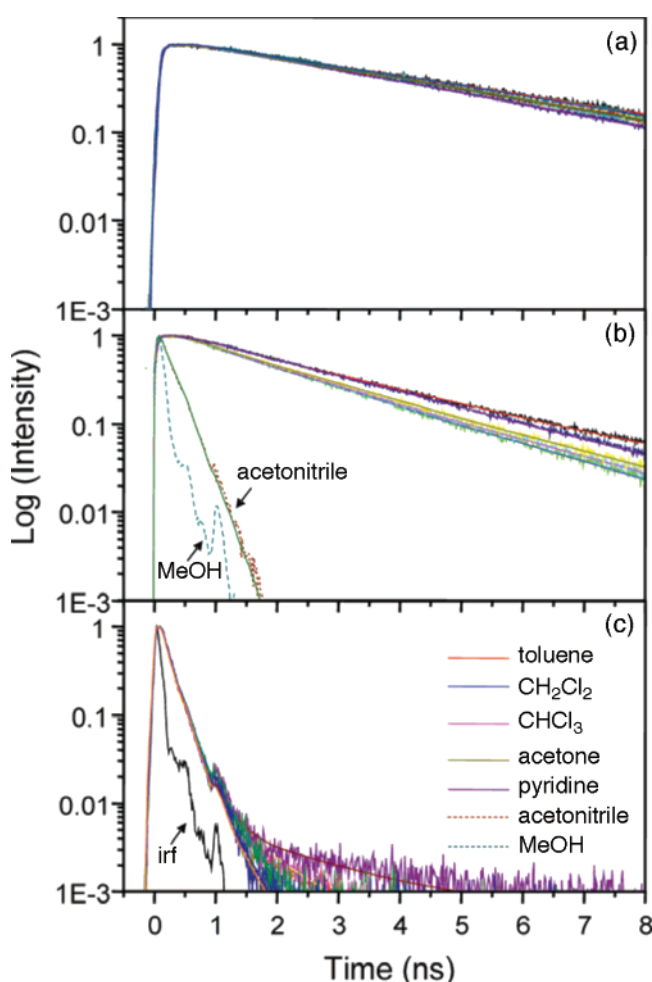


**Figure 10.** Fluorescence decay profiles of (a) **14g**, (b) **14e**, and (c) **14c** in seven solvents, where  $\lambda_{\text{ex}}$  is 390 nm and  $\lambda_{\text{em}}$ 's are detected at the maxima wavelengths. See Table 4.

Interestingly, the fluorescence decays of **14c** are very fast and nearly independent of solvents. However, we think that the fast decay of **14c** does not originate from the charge transfer

(34) Based on Hammett's rule, the electron-withdrawing abilities of 4-cyanophenyl and 4-nitrophenyl substituents are similar (only slightly larger in 4-nitrophenyl), but **14d** in acetonitrile or methanol showed no fluorescence-quenching behavior at any detection wavelengths (SI). It seems that the intramolecular charge transfer occurs only in **14e**.

but from the intersystem crossing from singlet to triplet excited state due to the heavy-atom effect induced by bromophenyl moieties. This is because the electron-donating power of 4-bromophenyl is weaker than that of 4-cyanophenyl, which does not show the fast component, based on Hammett's constant.<sup>35</sup>

## Summary

In summary, reliable synthetic routes toward *meso*-aryl-substituted subporphyrin **14** from pyridine–tri-*N*-pyrrolylborane (**12**), which allow the incorporation of a variety of *meso*-aryl substituents into the subporphyrin macrocycle, have been explored. X-ray crystallographic analysis revealed the bowl-shaped triangular structure of **14**, which provides enough space for the *meso*-phenyl ring to rotate freely. VT-NMR spectroscopy also supports the free rotation of *ortho*-nonsubstituted aromatic moieties even at  $-90$  °C on the NMR time scale. In contrast, such rotation is completely inhibited by methoxy groups on 2,6-positions. Importantly, substituents on the *meso*-phenyl rings have much larger influences on the electronic properties of the subporphyrin core, as compared to influences on those of porphyrins. Typically, the fluorescence spectrum and lifetime of **14e** are quite solvent-polarity dependent. Further investigation to tune-up properties of subporphyrins by *meso*-aryl substituents is now in progress.

## Experimental Section

**General Information.** All reagents and solvents were of commercial reagent grade and were used without further purification. <sup>1</sup>H, <sup>11</sup>B, <sup>13</sup>C, and <sup>19</sup>F NMR spectra were recorded on a JEOL delta-600 spectrometer, and chemical shifts were reported as the  $\delta$  scale in ppm relative to internal standards (CHCl<sub>3</sub> ( $\delta = 7.26$  ppm for <sup>1</sup>H, 77.16 ppm for <sup>13</sup>C), an external standard, BF<sub>3</sub>·OEt<sub>2</sub> in CDCl<sub>3</sub> ( $\delta = 0.00$  ppm for <sup>11</sup>B), and an external standard, C<sub>6</sub>F<sub>6</sub> in CDCl<sub>3</sub> ( $\delta = -162.9$  ppm for <sup>19</sup>F)). Spectroscopic grade solvents were used for all spectroscopic studies without further purification. UV/visible absorption spectra were recorded on a Shimadzu UV-3100 spectrometer. Fluorescence spectra were recorded on a Shimadzu RF-5300PC spectrometer with spectroscopic grade solvents. Relative fluorescence quantum yields were determined with a reference to that of 8-amino-1-naphthalenesulfonic acid ( $\Phi_f = 0.37$  in ethanol). ESI-TOF-MS spectra were recorded on a

(35) Klein, E.; Lukes, V. *J. Phys. Chem. A* **2006**, *110*, 12312–12320.

BRUKER DALTONICS micro TOF LC using positive-ion mode. Thin layer chromatography (TLC) was performed on a silica gel sheet, MERCK silica gel 60 F<sub>254</sub>. Preparative separations were performed by silica gel gravity column chromatography (Wako gel C-300) or size exclusion gel permeation chromatography (GPC) (Bio-Rad Bio-Beads S-X1, packed with THF in a 6 × 40 cm gravity column). Redox potentials were measured by the cyclic voltammetry method on an ALS electrochemical analyzer model 660.

Tri-*N*-pyrrolylborane (**9**) was prepared from borane–triethylamine complex and pyrrole by the reported procedure<sup>20a</sup> and was converted to pyridine–tri-*N*-pyrrolylborane (**12**) by treatment with pyridine under N<sub>2</sub> atmosphere.<sup>20b</sup> Both **9** and **12** are obtained as colorless solids.

**Protocol A for Preparing meso-Aryl-Substituted Subporphyrins 14.** To a suspension of pyridine–tri-*N*-pyrrolylborane (**12**) (500 mg, 1.74 mmol) in 1,2-dichlorobenzene (75 mL) were added aldehyde (5.22 mmol) and chloroacetic acid (173 mg, 1.83 mmol). The resulting mixture was refluxed for 1 h and then was cooled to room temperature. After the quenching of acid with triethylamine (0.20 mL, 1.5 mmol), the solvent was removed in vacuo. To the residual black tar, a mixture of THF/MeOH (1:1, 30 mL) was added and heated to 50 °C. After 10 min, the solvent was once evaporated, and the residue was mounted onto a GPC column (6 × 40 cm, THF) with a minimal amount of THF. Polymeric byproducts that eluted as the first fraction were removed, and the yellow fraction of subporphyrin **14** that emitted green fluorescence when excited by handy UV-light (at 365 nm) was carefully collected by checking TLC. Then, each subporphyrin was purified by the corresponding procedure described below.

**Protocol B for Preparing meso-Aryl-Substituted Subporphyrins 14.** To a suspension of pyridine–tri-*N*-pyrrolylborane (**12**) (500 mg, 1.74 mmol) in 75 mL of 1,2-dichlorobenzene was added aldehyde (5.22 mmol), and the mixture was cooled to 0 °C with an ice bath. After the dropwise addition of trifluoroacetic acid (0.139 mL, 1.80 mmol) via syringe, the solution was stirred for 1 h at 0 °C under N<sub>2</sub>. The acid was quenched with 0.15 mL of pyridine, and the resulting solution was heated to reflux. After 1 h, the solution was cooled to room temperature, and the solvent was removed in vacuo. To the residual black tar, a mixture of THF/MeOH (1:1, 30 mL) was added and heated to 50 °C. After 10 min, the solvent was once evaporated, and the residue was mounted onto a GPC column (6 × 40 cm, THF) with a minimal amount of THF. Polymeric byproducts that elute first were removed, and the yellow fraction of subporphyrin **14** that emits green fluorescence when excited by handy UV-light (at 365 nm) was carefully collected by checking TLC. Then, each subporphyrin was purified by the corresponding procedure described below.

**Methoxo(5,10,15-triphenylsubporphyrinato)boron(III) (14a).** According to protocol B, **14a** was prepared from **12** and benzaldehyde. The crude product was chromatographed on silica gel (eluent: CH<sub>2</sub>Cl<sub>2</sub>/hexane/ether = 1:2:1), and two yellow fractions that elute at *R<sub>f</sub>* = 0.54 and 0.25 were collected, which correspond to **14a** and **13a**, respectively. **13a** was converted again to **14a** by refluxing in a mixture of CH<sub>2</sub>Cl<sub>2</sub>/MeOH (2:1, 20 mL) for 10 min. Combined crude **14a** was further purified by silica gel column chromatography (eluent: CH<sub>2</sub>Cl<sub>2</sub>/hexane/ether = 1:3:1) and recrystallized from CH<sub>2</sub>Cl<sub>2</sub>/MeOH to give **14a** (33 mg, 3.8%) as orange solids. A single crystal suitable for X-ray diffraction analysis was prepared by slow recrystallization from CH<sub>2</sub>Cl<sub>2</sub>/methanol.

<sup>1</sup>H NMR (600 MHz, CDCl<sub>3</sub>) δ 8.12 (s, 6H, β), 8.06 (d, *J* = 7.8 Hz, 6H, Ph-*o*-H), 7.69 (pseudo t, *J* = 7.5 Hz, 6H, Ph-*m*-H), 7.61 (t, *J* = 7.3 Hz, 3H, Ph-*p*-H), and 0.82 (s, 3H, OMe); <sup>11</sup>B NMR (193 MHz, CDCl<sub>3</sub>) δ −15.3 (s, 1B); <sup>13</sup>C NMR (150 MHz, CDCl<sub>3</sub>) δ 141.1, 137.3, 133.3, 128.7, 127.9, 122.3, 120.7, and 46.9; HR-ESI TOF-MS *m/z* = 470.1833 (calcd for C<sub>33</sub>H<sub>21</sub>N<sub>3</sub>B<sub>1</sub> = 470.1829 [*M* − OMe]<sup>+</sup>); UV-vis (in CH<sub>2</sub>Cl<sub>2</sub>) λ [nm](ε [M<sup>−1</sup> cm<sup>−1</sup>]) 373(166000), 461(13000), and 484(9000). Fluorescence (in CH<sub>2</sub>Cl<sub>2</sub>, λ<sub>ex</sub> = 373 nm); λ<sub>max</sub> [nm] = 516, Φ<sub>F</sub> = 0.14.

**Methoxo(5,10,15-tri(4-*tert*-butylphenyl)subporphyrinato)boron(III) (14b).** According to protocol B, **14b** was prepared from **12** and 4-*tert*-butylbenzaldehyde. The crude product was chromatographed on silica gel (eluent: CH<sub>2</sub>Cl<sub>2</sub>/hexane/ether = 1:2:1), and two yellow fractions that elute at *R<sub>f</sub>* = 0.72 and 0.48 were collected, which correspond to **14b** and **13b**, respectively. **13b** was converted again to **14b** by refluxing in a mixture of CH<sub>2</sub>Cl<sub>2</sub>/MeOH (2:1, 20 mL) for 10 min. Combined crude **14b** was further purified by silica gel column chromatography (eluent: CH<sub>2</sub>Cl<sub>2</sub>/hexane/ether = 1:4:1) and recrystallized from CH<sub>2</sub>Cl<sub>2</sub>/MeOH to give **14b** (66 mg, 5.6%) as an orange crystalline solid. A single crystal suitable for X-ray diffraction analysis was prepared by slow recrystallization from CH<sub>2</sub>Cl<sub>2</sub>/methanol.

<sup>1</sup>H NMR (600 MHz, CDCl<sub>3</sub>) δ 8.13 (s, 6H, β), 8.00 (d, *J* = 8.2 Hz, 6H, aryl), 7.70 (d, *J* = 8.2 Hz, 6H, aryl), 1.49 (s, 27H, *tert*-butyl), and 0.80 (s, 3H, OMe); <sup>11</sup>B NMR (193 MHz, CDCl<sub>3</sub>) δ −15.2 (s, 1B); <sup>13</sup>C NMR (150 MHz, CDCl<sub>3</sub>) δ 150.8, 140.9, 134.5, 133.0, 125.7, 122.3, 120.5, 46.9, 34.9, and 31.6; HR-ESI TOF-MS *m/z* = 638.3693 (calcd for C<sub>45</sub>H<sub>45</sub>N<sub>3</sub>B<sub>1</sub> = 638.3709 [*M* − OMe]<sup>+</sup>); UV-vis (in CH<sub>2</sub>Cl<sub>2</sub>) λ [nm](ε [M<sup>−1</sup> cm<sup>−1</sup>]) 377(182000), 465(13000), and 491(14000). Fluorescence (in CH<sub>2</sub>Cl<sub>2</sub>, λ<sub>ex</sub> = 377 nm) λ<sub>max</sub> [nm] = 524, Φ<sub>F</sub> = 0.16.

**Methoxo(5,10,15-tri(4-bromophenyl)subporphyrinato)boron(III) (14c).** According to protocol B, **14c** was prepared from **12** and 4-bromobenzaldehyde. The crude product was chromatographed on silica gel (eluent: CH<sub>2</sub>Cl<sub>2</sub>/hexane/ether = 1:2:1), and two yellow fractions that elute at *R<sub>f</sub>* = 0.62 and 0.30 were collected, which correspond to **14c** and **13c**, respectively. **13c** was converted again to **14c** by refluxing in a mixture of CH<sub>2</sub>Cl<sub>2</sub>/MeOH (2:1, 20 mL) for 10 min. Combined crude **14c** was further purified by silica gel column chromatography (eluent: CH<sub>2</sub>Cl<sub>2</sub>/hexane/ether = 1:3:1) and recrystallized from CH<sub>2</sub>Cl<sub>2</sub>/MeOH to give **14c** (55 mg, 4.3%) as orange solids.

<sup>1</sup>H NMR (600 MHz, CDCl<sub>3</sub>) δ 8.09 (s, 6H, β), 7.90 (d, *J* = 8.7 Hz, 6H, aryl), 7.83 (d, *J* = 8.7 Hz, 6H, aryl), and 0.80 (s, 3H, OMe); <sup>11</sup>B NMR (193 MHz, CDCl<sub>3</sub>) δ −15.3 (s, 1B); <sup>13</sup>C NMR (150 MHz, CDCl<sub>3</sub>) δ 141.0, 136.0, 134.6, 132.0, 122.9, 122.4, 119.6, and 46.8; HR-ESI TOF-MS *m/z* = 707.9114 (calcd for C<sub>33</sub>H<sub>18</sub>N<sub>3</sub>B<sub>1</sub>Br<sub>3</sub> = 707.9108 [*M* − OMe]<sup>+</sup>); UV-vis (in CH<sub>2</sub>Cl<sub>2</sub>) λ [nm](ε [M<sup>−1</sup> cm<sup>−1</sup>]) 375(170000), 461(13000), and 487(11000). Fluorescence (in CH<sub>2</sub>Cl<sub>2</sub>, λ<sub>ex</sub> = 375 nm); λ<sub>max</sub> [nm] = 521, Φ<sub>F</sub> = 0.008.

**Trifluoroacetoxo(5,10,15-tri(4-bromophenyl)subporphyrinato)boron(III) (15c).** In a preparative scale, **14c** (5.0 mg, 6.8 μmol) was dissolved in a mixture of trifluoroacetic acid/dichloromethane (1:99, 10 mL), and the solvent was evaporated to dryness to give **15c** quantitatively. A single crystal of **15c** suitable for X-ray diffraction analysis was prepared by slow diffusion of trifluoroacetic acid into a dichloromethane solution of **14c**.

<sup>1</sup>H NMR (600 MHz, CDCl<sub>3</sub>) δ 8.18 (s, 6H, β), 7.93 (d, *J* = 8.2 Hz, 6H, aryl), and 7.86 (d, *J* = 8.2 Hz, 6H, aryl); <sup>11</sup>B NMR (193 MHz, CDCl<sub>3</sub>) δ −15.1 (broad s, 1B); <sup>19</sup>F NMR (565 MHz, CDCl<sub>3</sub>) δ −15.1 (s, 3F, OCOF<sub>3</sub>).

**Methoxo(5,10,15-tri(4-cyanophenyl)subporphyrinato)boron(III) (14d).** According to protocol B, **14d** was prepared from **12** and 4-cyanobenzaldehyde. The crude product was chromatographed on silica gel (eluent: CH<sub>2</sub>Cl<sub>2</sub>/ethyl acetate = 3:1), and two yellow fractions that elute at *R<sub>f</sub>* = 0.88 and 0.52 were collected, which correspond to **14d** and **13d**, respectively. **13d** was converted again to **14d** by refluxing in a mixture of CH<sub>2</sub>Cl<sub>2</sub>/MeOH (2:1, 20 mL) for 10 min. Combined crude **14d** was further purified by silica gel column chromatography (eluent: CH<sub>2</sub>Cl<sub>2</sub>/ethyl acetate = 5:1) and recrystallized from CH<sub>2</sub>Cl<sub>2</sub>/MeOH to give **14d** (35 mg, 3.5%) as an orange crystalline solid. A single crystal suitable for X-ray diffraction analysis was prepared by slow recrystallization from CH<sub>2</sub>Cl<sub>2</sub>/methanol.

<sup>1</sup>H NMR (600 MHz, CDCl<sub>3</sub>) δ 8.17 (d, *J* = 8.2 Hz, 6H, aryl), 8.12 (s, 6H, β), 8.01 (d, *J* = 8.2 Hz, 6H, aryl), and 0.79 (s, 3H, OMe); <sup>11</sup>B NMR (193 MHz, CDCl<sub>3</sub>) δ −15.4 (s, 1B); <sup>13</sup>C NMR (150 MHz, CDCl<sub>3</sub>) δ 141.6, 141.1, 133.7, 132.6, 122.7, 119.3, 118.8, 112.1, and 46.8; HR-ESI TOF-MS *m/z* = 545.1683 (calcd for C<sub>36</sub>H<sub>18</sub>N<sub>6</sub>B<sub>1</sub> = 545.1687 [*M*

– OMe]<sup>+</sup>); UV–vis (in CH<sub>2</sub>Cl<sub>2</sub>)  $\lambda$  [nm]( $\epsilon$  [M<sup>-1</sup> cm<sup>-1</sup>]) 380(192000) and 465(17000). Fluorescence (in CH<sub>2</sub>Cl<sub>2</sub>,  $\lambda_{\text{ex}}$  = 380 nm);  $\lambda_{\text{max}}$  [nm] = 522,  $\Phi_{\text{F}}$  = 0.17.

**Methoxo(5,10,15-tri(4-nitrophenyl)subporphyrinato)boron(III) (14e).** According to protocol B, **14e** was prepared from **12** and 4-nitrobenzaldehyde. The crude product was chromatographed on silica gel (eluent: CH<sub>2</sub>Cl<sub>2</sub>/ethyl acetate = 9:1), and two yellow fractions that elute at  $R_f$  = 0.76 and 0.38 were collected, which correspond to **14e** and **13e**, respectively. **13e** was converted again to **14e** by refluxing in a mixture of CH<sub>2</sub>Cl<sub>2</sub>/MeOH (2:1, 20 mL) for 10 min. Combined crude **14e** was further purified by silica gel column chromatography (eluent: CH<sub>2</sub>Cl<sub>2</sub>/ethyl acetate = 20:1) and recrystallized from CH<sub>2</sub>Cl<sub>2</sub>/MeOH to give **14e** (31 mg, 2.8%) as a reddish-orange crystalline solid. A single crystal suitable for X-ray diffraction analysis was prepared by slow recrystallization from chloroform/methanol.

<sup>1</sup>H NMR (600 MHz, CDCl<sub>3</sub>)  $\delta$  8.60 (d,  $J$  = 8.7 Hz, 6H, aryl), 8.23 (d,  $J$  = 8.7 Hz, 6H, aryl), 8.16 (s, 6H,  $\beta$ ), and 0.83 (s, 3H, OMe); <sup>11</sup>B NMR (193 MHz, CDCl<sub>3</sub>)  $\delta$  –15.4 (s, 1B); <sup>13</sup>C NMR (150 MHz, CDCl<sub>3</sub>)  $\delta$  147.9, 143.5, 141.3, 133.8, 124.1, 122.9, 119.1, and 46.9; HR-ESI TOF-MS  $m/z$  = 605.1379 (calcd for C<sub>33</sub>H<sub>18</sub>N<sub>6</sub>B<sub>1</sub>O<sub>6</sub> = 605.1381 [M – OMe]<sup>+</sup>); UV–vis (in CH<sub>2</sub>Cl<sub>2</sub>)  $\lambda$  [nm]( $\epsilon$  [M<sup>-1</sup> cm<sup>-1</sup>]) 397(110000), 471-(18000), and 492 (16000); UV–vis (in MeOH)  $\lambda$  [nm]( $\epsilon$  [M<sup>-1</sup> cm<sup>-1</sup>]) 389(138000) and 468(19000). Fluorescence (in CH<sub>2</sub>Cl<sub>2</sub>,  $\lambda_{\text{ex}}$  = 397 nm)  $\lambda_{\text{max}}$  [nm] = 543,  $\Phi_{\text{F}}$  = 0.15. Fluorescence (in MeOH,  $\lambda_{\text{ex}}$  = 389 nm)  $\lambda_{\text{max}}$  [nm] = 530,  $\Phi_{\text{F}}$  = 0.002.

**Methoxo(5,10,15-tris(3,4,5-trimethoxyphenyl)subporphyrinato)boron(III) (14f).** According to protocol B, **14f** was prepared from **12** and 3,4,5-trimethoxybenzaldehyde. The crude product was chromatographed on silica gel (eluent: CH<sub>2</sub>Cl<sub>2</sub>/ethyl acetate = 2:1), and two yellow fractions that elute at  $R_f$  = 0.68 and 0.45 were collected, which correspond to **14f** and **13f**, respectively. **13f** was converted again to **14f** by refluxing in a mixture of CH<sub>2</sub>Cl<sub>2</sub>/MeOH (2:1, 20 mL) for 10 min. Combined crude **14f** was further purified by silica gel column chromatography (eluent: CH<sub>2</sub>Cl<sub>2</sub>/ethyl acetate = 3:1) and recrystallized from CH<sub>2</sub>Cl<sub>2</sub>/MeOH to give **14f** (75 mg, 5.6%) as orange solids.

<sup>1</sup>H NMR (600 MHz, CD<sub>2</sub>Cl<sub>2</sub>)  $\delta$  8.15 (s, 6H,  $\beta$ ), 7.25 (s, 6H, aryl-*o*-H), 4.05 (s, 18H, aryl-*m*-OMe), 3.99 (s, 9H, aryl-*p*-OMe), and 0.86 (s, 3H, axial-OMe); <sup>11</sup>B NMR (193 MHz, CDCl<sub>3</sub>)  $\delta$  –15.2 (s, 1B); <sup>13</sup>C NMR (150 MHz, CDCl<sub>3</sub>)  $\delta$  153.4, 141.2, 138.4, 132.7, 122.4, 120.8, 110.8, 61.3, 56.6, and 47.0; HR-ESI TOF-MS  $m/z$  = 740.2771 (calcd for C<sub>42</sub>H<sub>39</sub>N<sub>3</sub>B<sub>1</sub>O<sub>9</sub> = 740.2781 [M – OMe]<sup>+</sup>); UV–vis (in CH<sub>2</sub>Cl<sub>2</sub>)  $\lambda$  [nm]( $\epsilon$  [M<sup>-1</sup> cm<sup>-1</sup>]) 380(176000), 464(13000), and 493(15000). Fluorescence (in CH<sub>2</sub>Cl<sub>2</sub>,  $\lambda_{\text{ex}}$  = 380 nm)  $\lambda_{\text{max}}$  [nm] = 538,  $\Phi_{\text{F}}$  = 0.12.

**Methoxo(5,10,15-tris(2,4,6-trimethoxyphenyl)subporphyrinato)boron(III) (14g).** According to protocol A, to a suspension of pyridine–tri-*N*-pyrrolylborane (**12**) (500 mg, 1.74 mmol) in 1,2-dichlorobenzene 100 mL were added 2,4,6-trimethoxybenzaldehyde (3.06 g, 15.6 mmol) and chloroacetic acid (173 mg, 1.83 mmol). The reaction solution was heated to reflux in the dark, open to air. After refluxing for 2.5 h, the resulting dark solution was cooled to room temperature with a water bath, and then the acid was quenched with triethylamine (0.20 mL, 1.5 mmol). The resulting solution was directly poured on top of a silica gel column (6 × 15 cm) packed with CH<sub>2</sub>Cl<sub>2</sub>. First, 1,2-dichlorobenzene was eluted with CH<sub>2</sub>Cl<sub>2</sub>, and then **13g** was eluted with CH<sub>2</sub>Cl<sub>2</sub>/ethyl acetate = 2:1 ( $R_f$  = 0.15). From the crude mixture of **13g**, polymeric byproducts were removed by GPC column chromatography (4 × 60 cm, eluent: THF), and roughly isolated **13g** was converted to **14g** by refluxing in a mixture of CH<sub>2</sub>Cl<sub>2</sub>/MeOH (2:1, 20 mL) for 10 min. Crude **14g** was further purified by silica gel column chromatography (eluent: CH<sub>2</sub>Cl<sub>2</sub>/ethyl acetate = 2:1,  $R_f$  = 0.32). The obtained yellow fraction was recrystallized from CH<sub>2</sub>Cl<sub>2</sub>/MeOH to give orange solids of **14g** (14.4 mg, 1.1%) as a yellowish-orange crystalline solid. A single crystal suitable for X-ray diffraction analysis was prepared by slow recrystallization from chloroform/methanol.

<sup>1</sup>H NMR (600 MHz, CD<sub>2</sub>Cl<sub>2</sub>)  $\delta$  7.63 (s, 6H,  $\beta$ ), 6.50 (d,  $J$  = 2.3 Hz, 3H, aryl-*m*-H), 6.32 (d,  $J$  = 2.3 Hz, 3H, aryl-*m*-H), 3.98 (s, 9H, aryl-*p*-OMe), 3.79 (s, 9H, aryl-*o*-OMe), 3.32 (s, 9H, aryl-*o*-OMe), and 0.95 (s, 3H, axial-OMe); <sup>11</sup>B NMR (193 MHz, CDCl<sub>3</sub>)  $\delta$  –15.2 (s, 1B); <sup>13</sup>C NMR (150 MHz, CDCl<sub>3</sub>)  $\delta$  162.0, 161.8, 159.4, 142.0, 120.3, 111.3, 107.3, 91.3, 91.0, 56.5, 55.6, 55.2, and 46.5; HR-ESI TOF-MS  $m/z$  = 740.2787 (calcd for C<sub>42</sub>H<sub>39</sub>N<sub>3</sub>B<sub>1</sub>O<sub>9</sub> = 740.2781 [M – OMe]<sup>+</sup>); UV–vis (in CH<sub>2</sub>Cl<sub>2</sub>)  $\lambda$  [nm]( $\epsilon$  [M<sup>-1</sup> cm<sup>-1</sup>]) 372(156000) and 454-(17000). Fluorescence (in CH<sub>2</sub>Cl<sub>2</sub>,  $\lambda_{\text{ex}}$  = 372 nm)  $\lambda_{\text{max}}$  [nm] = 524,  $\Phi_{\text{F}}$  = 0.11.

**X-ray Diffraction Analysis. Crystallographic data for 14a:** C<sub>34</sub>H<sub>24</sub>BN<sub>3</sub>O,  $M_r$  = 501.37, monoclinic, space group  $P2_1/c$ ,  $a$  = 14.220(5) Å,  $b$  = 13.712(5) Å,  $c$  = 25.833(9) Å,  $\beta$  = 100.282(14)°,  $V$  = 4956(3) Å<sup>3</sup>,  $Z$  = 8,  $D_{\text{calc}}$  = 1.344 g cm<sup>-3</sup>,  $R_1$  = 0.0769 for  $I > 2\sigma(I)$ ,  $wR_2$  = 0.2266 for all data, GOF = 1.066, CCDC 630975.

**Crystallographic data for 14b:** C<sub>46</sub>H<sub>48</sub>BN<sub>3</sub>O·2(CH<sub>4</sub>O),  $M_r$  = 733.77, monoclinic, space group  $C2/c$ ,  $a$  = 28.712(2) Å,  $b$  = 16.7407(13) Å,  $c$  = 22.2837(17) Å,  $\beta$  = 130.0030(10)°,  $V$  = 8204.6(11) Å<sup>3</sup>,  $Z$  = 8,  $D_{\text{calc}}$  = 1.188 g cm<sup>-3</sup>,  $R_1$  = 0.0675 for  $I > 2\sigma(I)$ ,  $wR_2$  = 0.1881 for all data, GOF = 1.028, CCDC 630976.

**Crystallographic data for 15c:** C<sub>35</sub>H<sub>18</sub>BBr<sub>3</sub>F<sub>3</sub>N<sub>3</sub>O<sub>2</sub>,  $M_r$  = 820.06, triclinic, space group  $P\bar{1}$ ,  $a$  = 9.892(4) Å,  $b$  = 13.130(5) Å,  $c$  = 13.752(5) Å,  $\alpha$  = 61.550(15)°,  $\beta$  = 83.001(16)°,  $\gamma$  = 80.696(17)°,  $V$  = 1533.6(10) Å<sup>3</sup>,  $Z$  = 2,  $D_{\text{calc}}$  = 1.776 g cm<sup>-3</sup>,  $R_1$  = 0.0467 for  $I > 2\sigma(I)$ ,  $wR_2$  = 0.1617 for all data, GOF = 1.087, CCDC 630977.

**Crystallographic data for 14d:** C<sub>37</sub>H<sub>21</sub>BN<sub>3</sub>O,  $M_r$  = 576.41, monoclinic, space group  $P2_1/a$ ,  $a$  = 8.017(7) Å,  $b$  = 21.24(2) Å,  $c$  = 16.75(2) Å,  $\beta$  = 90.28(5)°,  $V$  = 2852(5) Å<sup>3</sup>,  $Z$  = 4,  $D_{\text{calc}}$  = 1.342 g cm<sup>-3</sup>,  $R_1$  = 0.0854 for  $I > 2\sigma(I)$ ,  $wR_2$  = 0.2036 for all data, GOF = 1.023, CCDC 630978.

**Crystallographic data for 14e:** 4(C<sub>34</sub>H<sub>21</sub>BN<sub>3</sub>O<sub>7</sub>)·3(CHCl<sub>3</sub>),  $M_r$  = 2903.60, triclinic, space group  $P\bar{1}$ ,  $a$  = 14.2905(11) Å,  $b$  = 14.3984(12) Å,  $c$  = 16.4038(13) Å,  $\alpha$  = 79.2060(10)°,  $\beta$  = 81.2920(10)°,  $\gamma$  = 73.630(2)°,  $V$  = 3163.7(4) Å<sup>3</sup>,  $Z$  = 1,  $D_{\text{calc}}$  = 1.524 g cm<sup>-3</sup>,  $R_1$  = 0.0479 for  $I > 2\sigma(I)$ ,  $wR_2$  = 0.1327 for all data, GOF = 1.039, CCDC 630979.

**Crystallographic data for 14g:** C<sub>43</sub>H<sub>42</sub>BN<sub>3</sub>O<sub>10</sub>·C<sub>1.56</sub>H<sub>4.93</sub>Cl<sub>1.31</sub>O<sub>1.12</sub>·C<sub>0.56</sub>H<sub>2.22</sub>O<sub>1.44</sub>,  $M_r$  = 916.17, triclinic, space group  $P\bar{1}$ ,  $a$  = 12.6630(11) Å,  $b$  = 14.0703(13) Å,  $c$  = 14.9534(13) Å,  $\alpha$  = 111.674(2)°,  $\beta$  = 103.125(2)°,  $\gamma$  = 101.496(2)°,  $V$  = 2290.2(4) Å<sup>3</sup>,  $Z$  = 2,  $D_{\text{calc}}$  = 1.329 g cm<sup>-3</sup>,  $R_1$  = 0.0724 for  $I > 2\sigma(I)$ ,  $wR_2$  = 0.1978 for all data, GOF = 1.032, CCDC 630980.

**Time-Correlated Single Photon Counting.** Time-resolved fluorescence was detected using a time-correlated single photon counting (TCSPC) technique. A homemade cavity-dumped Ti:Sapphire oscillator pumped by a CW Nd:YVO<sub>4</sub> laser (Coherent, Verdi) was used as the excitation light source; this provided ultrashort pulses (100 fs at full width half-maximum [fwhm]) and allowed for a high repetition rate (200–400 kHz). The output pulse of the oscillator was frequency doubled with a second harmonic crystal. The TCSPC detection system consisted of a multichannel plate photomultiplier (Hamamatsu, R3809U-51) with a cooler (Hamamatsu, C4878), a TAC (time-to-amplitude converter) (EG&G Ortec, 457), two discriminators (EG&G Ortec, 584 (signal) and Canberra, 2126 (trigger)), and two wideband amplifiers (Philip Scientific (signal) and a Mini Circuit (trigger)). A personal computer with a multichannel analyzer (Canberra, PCA3) was used for data storage and processing. The overall instrumental response function was about 60 ps (fwhm). The decay fittings were made by using a least-squares deconvolution fitting process (LIFETIME program with an iterative nonlinear least-squares deconvolution procedure developed at the University of Pennsylvania).<sup>32</sup>

**Acknowledgment.** The work at Kyoto was partly supported by a Grant-in-Aid (B) (No. 17350017) from Ministry of Education, Culture, Sports, Science and Technology, Japan, by

21st Century COE on Kyoto University Alliance for Chemistry, and by CREST (Core Research for Evolutional Science and Technology) of Japan Science and Technology Agency (JST). The work at Yonsei was supported by the Star Faculty Program of the Ministry of Education and Human Resources Development, Korea. ZSY thanks the fellowship of the BK 21 program from the Ministry of Education and Human Resources

Development, Korea. Y.I. thanks the JSPS fellowship for Young Scientists.

**Supporting Information Available:** Complete ref 25a; experimental details. This material is available free of charge via the Internet at <http://pubs.acs.org>.

JA069324Z